American Mineralogist, Volume 78, pages 533–557, 1993

Structural characterization of kerogens to granulite-facies graphite: Applicability of Raman microprobe spectroscopy

Brigitte Wopenka, Jill Dill Pasteris
Washington University, Department of Earth and Planetary Sciences, One Brookings Drive, Campus Box 1169, St. Louis, Missouri 63130-4899, U.S.A.

Abstract

The usefulness of the laser Raman microprobe (LRM) in characterizing the state of structural order of geologically relevant carbonaceous materials (CM) ranging from kerogen and coals to granulite-facies graphite (in our samples, 4 Å $< L_a < \infty$) is demonstrated. The first part of this paper is an overview of the process of graphitization, two techniques used to characterize CM structurally (HRTEM and XRD analysis), and the theory of Raman spectroscopic analysis of CM. The first- and second-order Raman spectra of 37 CM samples are presented: 24 grain separates from various metamorphic terranes (chlorite zone to granulite facies), eight kerogen and coal separates, two thin sections containing graphite, and three artificial fluid-deposited CM. The results are evaluated and discussed in terms of (1) various quantitative spectral parameters such as the positions, widths, height ratios, and area ratios of Raman peaks resulting from ordered and disordered materials, and (2) estimates of the in-plane crystallite size, L_a, based on the existing calibration data from XRD (Tuinstra and Koenig, 1970a) and HRTEM (Beny-Bassez and Rouzaud, 1985). We conclude that LRM spectroscopy is very well suited to the characterization of CM of geological interest, because the spectra allow one to distinguish different stages of crystallite development (even for very poorly and very well crystallized CM) more accurately than do quantitative routine XRD data and because the Raman spectra are more representative of the bulk carbonaceous sample than are HRTEM data. Our Raman results suggest that the mechanism and developmental stages of graphitization are basically the same for all (artificial, as well as natural) heat-treated CM once some low threshold of three-dimensional ordering is reached. It appears, however, that fluid-deposited CM may develop differently than heat-treated CM. Specific information is provided on the thermal response of metapelite-hosted CM, and the geological implications of identifying disordered CM ("graphite") in situ are discussed.

Introduction

Various forms of solid carbonaceous material (CM) make up a significant proportion of the Earth's crust (≈0.03 wt%, based on data from Tissot and Welte, 1984), as well as many extraterrestrial objects (Tarter et al., 1990). These materials range from coal and kerogens to highly crystalline graphite on Earth, as well as from poorly to highly crystalline carbonaceous matter in meteorites and interplanetary dust particles (e.g., Allamandola et al., 1987; Wopenka, 1988; Macklin et al., 1990; Zinner et al., 1990). Depending on its relative abundance and reactivity, CM can act as a buffer or indicator of f_{O_2} in an assemblage with which it is in equilibrium (e.g., Miyashiro, 1964; French, 1964, 1966; Ziegenbein and Johannes, 1980; Holloway, 1984). Unraveling and interpreting the structural and compositional subtleties and complexities of CM is very important in the interpretation of the degree of metamorphism of its host rock and for thermodynamic calculations involving reduced C phases. For instance, in cases in which the f_{O_2} of a system is buffered by graphite-bearing assemblages, any deviation from pure C, well-crystallized graphite produces a shift in the calculated f_{O_2} compared with that for the idealized reaction (e.g., Ziegenbein and Johannes, 1990). In addition, both the degree of crystallinity of graphite (French, 1964; Landis, 1971; Grew, 1974; Itaya, 1981; Wedeking and Hayes, 1983) and the C isotopic fractionation between graphite and carbonate (Bottinga, 1969; Valley and O'Neil, 1981; Arneth et al., 1985; Dunn and Valley, 1988, 1992; Hoefs et al., 1988; Chacko et al., 1991) have been used to infer the degree of metamorphism and temperature of equilibration of a wide range of rock types.

Both of the latter geothermometric methods require that the CM be well characterized. It has been recognized for many years that Raman spectroscopy can provide information on the degree of crystallinity of CM that is complementary to the information obtained from XRD and HRTEM techniques (Tuinstra and Koenig, 1970a, 1970b; Beny-Bassez and Rouzaud, 1985). However, most previous Raman studies dealing with the question of the degree of crystallinity of CM were done on synthetic or-

0003–004X/93/0506–0533$02.00

ganic compounds that are not necessarily good analogues to naturally occurring carbonaceous matter. Only with the advent of laser Raman microprobes has Raman spectroscopy been applied effectively, but not yet in a large number of studies, to CM of geological origin (e.g., Guilhaumou et al., 1984; Beny-Bassez and Rouzaud, 1985; Pasteris et al., 1986; Hess et al., 1988; Pasteris and Wanamaker, 1988; Wopenka and Pasteris, 1988; Wopenka et al., 1988; Wang et al., 1989; Landais et al., 1990; Pasteris and Wopenka, 1991; Reutel, 1992).

This paper addresses the interpretation of Raman spectra obtained on natural terrestrial carbonaceous materials ranging from kerogens to granulite-facies graphite. For samples from a suite of regionally metamorphosed C-bearing pelites, the Raman spectroscopic results from this study are compared with those from XRD (Grew, 1974) and HRTEM (Buseck and Huang, 1985). For a suite of kerogens, Raman spectroscopic data (this study), HRTEM observations (Buseck et al., 1988), and XRD data and results from bulk compositional analyses (Hayes et al., 1983) are compared. In addition, Raman spectra of coal and of CM hosted in marble, granofels, and metaflysch, as well as CM deposited from various fluids under specified conditions, are discussed.

Process of graphitization

The two major processes that give rise to the formation of graphite in terrestrial rocks are (1) the saturation of a fluid with respect to a solid C phase, and (2) the transformation of organic matter, by means of heat (± pressure), into a C-dominated solid. Process 1, i.e., fluid deposition, accounts for numerous graphite vein deposits (e.g., in Duluth Complex: Hollister, 1980; in Sri Lanka: Katz, 1987; in New Hampshire: Rumble and Hoering, 1986; in Ivrea Zone: Baker, 1988), associations of graphite with hydrously altered silicates (in New Hampshire: Duke and Rumble, 1986; in Bushveld Complex: Ballhaus and Stumpfl, 1985; in Duluth Complex: Sassani and Pasteris, 1988), and graphitic particulates adjacent to hydrothermal vents on the sea floor (Jedwab and Boulegue, 1984). There is much more analytical information available on graphitic materials that are derived by means of process 2, i.e., from organic precursors. This paper concentrates on the latter but also provides Raman data on several examples of fluid-deposited CM.

The chemical conversion of organic material (solid, liquid, or gas) and the physical transformation of disordered carbonaceous matter into well-ordered, pure carbon graphite will be referred to here as graphitization. Both compositional and structural changes are involved in the graphitization process, which proceeds along two paths: within the C layers (sheet formation) and perpendicular to them (stack formation). The degree of crystallinity of graphite therefore is evaluated in terms of in-plane crystallite size (L_a) and stacking height (L_c), as well as interplanar d values. Once it is established during graphitization, the hexagonal planar geometry (i.e., bond lengths and bond angles) of the aromatic layers remains unchanged. Further structural organization during graphitization manifests itself in a reduction of d values and in an increase of both L_a and L_c. The latter define the size of the crystallite (but not the particle size; a graphite particle or grain may consist of many crystallites) and represent average scales of coherent domains of organization. Well-crystallized graphite is defined by an interplanar d value of exactly 3.35 Å and is on the order of at least several hundreds to a thousand ångströms for each L_a and L_c.

In nature, not only temperature, but also pressure, shear, catalytic species, type of hydrocarbon precursors, and time influence the graphitization process (e.g., Bonijoly et al., 1982; Ross and Bustin, 1990). However, some analogies between synthetic and natural graphitic materials seem to be valid. Ergun (1968) and Rouzaud et al. (1983), for instance, agreed in their findings that three-dimensional ordering begins at a relatively early stage of crystallite growth, i.e., when L_a attains a size of only about 30 Å. In addition, temperature-incremented experiments on synthetic CM show that L_a increases from 30 to 350 Å over a temperature interval of only 400 °C. Geological materials commonly undergo this range of thermal change. However, the actual temperature of transition to well-ordered graphite is different for synthetic highly oriented pyrolytic graphite (HOPG; between 1600 and 2600 °C, depending on the carbonaceous precursor: Kelly, 1981; Rouzaud et al., 1983) than for natural graphite (according to Landis, 1971; Dunn and Valley, 1992; and Grew, 1974, well-crystallized graphite can occur in rocks that were never heated above 450, 500, and 650 °C, respectively).

Methods for studying structural order in carbonaceous materials

A major concern in the geothermometric interpretation of CM is how to evaluate its degree of ordering, or degree of crystallinity. "Disorder" in CM refers to structural deviations from the well-defined, three-dimensional crystal structure of graphite. As explained above, however, ordering may occur at different rates along the various crystallographic directions. This leads to confusion and inconsistency with the order-disorder nomenclature, because the evolution of order can be monitored in two different aspects of crystallite size (L_a, L_c), as well as in interplanar d values. The various analytical techniques used to characterize carbonaceous materials involve optical reflectance measurements (vitrinite reflectance: e.g., Diessel and Offler, 1975; Diessel et al., 1978; Okuyama-Kusunose and Itaya, 1987), infrared spectroscopy (e.g., Rouzaud et al., 1991), neutron diffraction scattering (e.g., Mildner and Carpenter, 1982), measurements of magnetic properties (e.g., Rouzaud et al., 1991), XRD, HRTEM, and Raman spectroscopy, of which the latter three are discussed in more detail below (see also Table 1).

X-ray diffractometry

In routine XRD experiments, the (002) reflection (for ordered graphite, $2\theta = 26.5°$ for Cu$K\alpha$ radiation) is mea-

Table 1. Comparison of methods for structural characterization of graphite

	XRD	HRTEM	Raman
Sample preparation	destructive: bulk separates	destructive: bulk separates	nondestructive: in situ in thin sections or rock powders
Size of sample	bulk technique	hundreds of ångströms	μm^3
Scale	macro	micro	mini
Crystallite dimension measured	d (L_c, L_a)	d, L_c, L_a	L_a (L_c)
Information about crystallite size	indirect	direct	indirect
Analysis time	slow because of required sample preparation	very slow because of scale and complexity of analysis	relatively fast because of minimal sample preparation and scale of analysis

sured, which gives information on the interplanar d values (derived from peak position) and on stacking height L_c (derived from peak width). Generally speaking, the wider the (002) peak, the smaller L_c. In principle, the third important parameter for the structural characterization of graphite, L_a, also can be derived from XRD analysis (Ergun, 1968). The in-plane crystallite size L_a can be estimated from the width of the (110) reflection (at $2\theta = 77.5°$ for Cu$K\alpha$). It is the latter parameter that was presumably used by Tuinstra and Koenig (1970a) to calibrate Raman spectra of CM in terms of L_a (see discussion below). Determinations of L_c and L_a are seldom made by means of XRD, however, because the peak widths are also strongly dependent on the grain size distribution and the grain orientation (e.g., Wintsch et al., 1981), as well as on various instrumental effects (Ergun, 1968), and thus are difficult to interpret unambiguously (see discussion). The most straightforward use of XRD analysis is the calculation of the d values, which readily distinguishes well-crystallized graphite ($d = 3.35$ Å) from disordered carbonaceous material ($d > 3.35$ Å). XRD usually is done on bulk graphitic materials that have been separated and concentrated from ground rock samples, either by acid dissolution of their matrix or by H_2O flotation. One disadvantage of the XRD technique, therefore, is that the rock must be disaggregated, thereby physically disrupting and perhaps altering the graphite, as well as destroying textural relationships in the sample. Furthermore, characterization is provided for the bulk material, with little ability to reflect the range of properties or the degree of heterogeneity of the sample.

High-resolution transmission electron microscopy

Analysis by HRTEM lies at the opposite end of the spectrum of sample sizes from XRD analysis (see Table 1). HRTEM typically permits investigation of CM on the scale of hundreds of ångströms. However, depending on the desired information and the resolution required to obtain it, imaging of sample domains up to a few micrometers is possible. Lattice-fringe and dark-field images permit direct observation and measurement of the dimension of stacks (L_c), the interfringe spacings (d), the planarity of fringes, and the abundance of defects, such as edge dislocations, as well as the lateral extent of C sheets, L_a (e.g., Oberlin et al., 1980; Rouzaud et al., 1983; Buseck et al., 1987; Deurbergue et al., 1987; Wang et al., 1989; Oh et al., 1991). Beny-Bassez and Rouzaud (1985) measured (110) dark-field images to calibrate Raman spectra of CM in terms of L_a (see discussion below). The appearance (smeared or discrete) of rings and spots in electron and optical diffraction patterns further aid the characterization of structural perfection and the calculation of interlayer d values. Although the HRTEM technique yields excellent information on structure (and, if additional X-ray detection capabilities are available, also on composition), it also has several drawbacks. As for XRD analysis, the CM first must be disaggregated from its matrix. For analysis in a transmission electron microscope, the sample frequently must be thinned or smeared, disrupting the coarser scale textural and crystallographic integrity of the CM particles. As a result, it is not known whether observed layer imperfections are true growth features or were produced during sample preparation (Buseck and Huang, 1985). Furthermore, impurities naturally incorporated into carbonaceous material could be dissolved and removed during sample preparation, thus eliminating them from analysis. Another limitation is that the production of high-quality HRTEM images on samples with such small interplanar spacings requires extremely high standards in both the expertise of the operator and the alignment and performance of the instrument.

Raman spectroscopy

The lattice dynamics of graphite have been treated theoretically in numerous publications. Several approaches have been used to model the experimentally obtained Raman spectra (e.g., Nemanich and Solin, 1979; Lespade et al., 1982). The first Raman scattering studies of graphite were carried out by Tuinstra and Koenig (1970a, 1970b). Their original peak assignments have been updated with new findings and interpretations, which are summarized in Dresselhaus and Dresselhaus (1982) and in other articles. Some of the points important to the interpretation of Raman spectra of naturally occurring CM are discussed below.

Among the 12 zone-center optical lattice modes in well-crystallized graphite (space group $D^4_{6h} = P6_3/mmc$, hexagonal Brillouin zone), only two in-plane modes (E_{2g1} and E_{2g2}, both of which are degenerate) are Raman active.

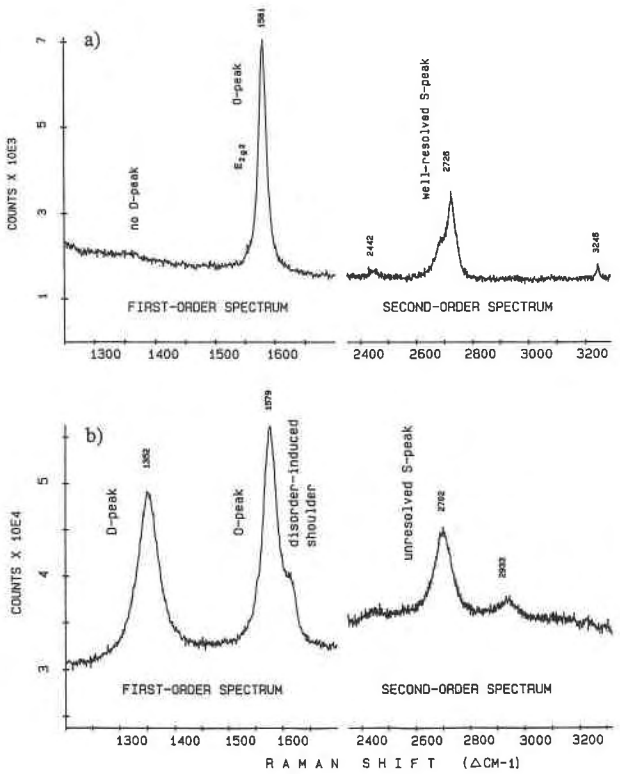

Fig. 1. (a) First- and second-order Raman spectra of well-crystallized graphite, with "infinite" in-plane crystallite size L_a (see text). Spectral windows scanned for first- and second-order Raman bands are 1200–1700 and 2350–3350 cm^{-1}, respectively. O peak at $\approx$1600 cm^{-1} is due to first-order E_{2g2} Raman band; D peak at $\approx$1355 cm^{-1} is due to disorder-induced first-order Raman band; S peak at $\approx$2715 cm^{-1} is caused by main second-order Raman band. Sample (entry no. 29, Table 2) from hydrously altered troctolite at the base of the Duluth Complex, Minnesota. (b) First- and second-order Raman spectra of a microcrystalline (disordered) form of carbonaceous material. Additional disorder-induced bands (cf. a) are due to breakdown of theoretical wave vector selection rules (see text). Sample no. 71-78 (entry no. 4, Table 2) hosted in metapelite from chlorite zone.

One of those modes is so low in frequency (E_{2g1} at 42 cm^{-1}) that in practice it cannot be resolved from Rayleigh scattering. Thus, it is the E_{2g2} mode at 1582 $\pm$ 1 cm^{-1} (Fig. 1a) that is observed in the first-order Raman spectrum of well-crystallized graphite. In models of Raman scattering, the theoretical wave-vector selection rules hold for crystals of infinite in-plane crystallite size, L_a. Graphite shows an unusual phenomenon, however: the wave-vector selection rules break down as the in-plane crystallite size L_a decreases below some minimum value, which allows the light-scattering process to occur from phonons outside the zone center of the phonon dispersion curves determined for well-crystallized graphite (e.g., Lespade et al., 1982). The graphitic structure becomes disordered in the Raman spectroscopic sense, as reflected in observable features in both the first-order and second-order Raman spectra (Fig. 1b, cf. Fig. 1a).

The above considerations explain the additional disorder-induced bands that appear in the Raman spectra of microcrystalline forms of CM (see Fig. 1b). These bands correspond to maxima in the phonon density of states (Nemanich and Solin, 1979). The major modifications in the first-order spectrum that arise from a decrease in crystallite size L_a are the development of a shoulder ($\approx$1622 cm^{-1}) on the high-wavenumber side of the $\approx$1582-cm^{-1} ("ordered," or O) peak and the appearance of a strong ("disordered," or D) peak at $\approx$1355 cm^{-1}. In very disordered graphite, the $\approx$1582- and the $\approx$1622-cm^{-1} peaks cannot be resolved, and they instead may produce a single broad peak at $\approx$1600 cm^{-1} (Fig. 2A, top). Tuinstra and Koenig (1970a) and Beny-Bassez and Rouzaud (1985) independently studied the relationship between the first-order Raman spectrum of CM and its in-plane crystallite size, L_a, as determined by means of XRD and HRTEM analysis, respectively (see discussion below). Although such facts frequently are ignored in the applied Raman literature, (1) the first-order spectra are also sensitive to stacking phenomena such as intercalation (e.g., Dresselhaus and Dresselhaus, 1982), and (2) information on three-dimensional ordering in CM is reflected in its second-order spectrum (Lespade et al., 1982, 1984). The latter actually can be quite useful in distinguishing among different stages of graphitization, e.g., the final stages of graphitization are best recognized from the second-, rather than the first-order spectrum.

Second-order bands theoretically can be modeled as two-phonon modes. Lattice-symmetry analysis for graphite does not predict lines at high frequencies, which probably accounts for their neglect by Tuinstra and Koenig (1970a). Indeed, the second-order bands of CM were not described until the late 1970s (e.g., Vidano and Fischbach, 1978). The theoretical identification of the second-order bands is made using the density of phonon states; maxima occur at 1620, 1360, and 830 cm^{-1} (Elman et al., 1981). The second-order Raman bands are assigned both to overtone scattering (2 $\times$ 1360 cm^{-1} $\approx$ 2735 cm^{-1}, the most intense second-order peak, designated here as the S peak, see below; 2 $\times$ 1620 cm^{-1} $\approx$ 3248 cm^{-1}, a weak, but sharp peak) and combination scattering (1620 cm^{-1} + 830 cm^{-1} $\approx$ 2450 cm^{-1}; 1620 cm^{-1} + 1355 cm^{-1} or 1580 cm^{-1} + 1355 cm^{-1} $\approx$ 2950 cm^{-1}). The reasons for the exact peak positions, intensity ratios, and band structures of the observed and calculated second-order Raman peaks are discussed extensively in the solid-state literature (e.g., Nemanich and Solin, 1979; Elman et al., 1981, 1982). However, in practice, we always have observed the S peak at much lower wavenumbers than predicted (see Table 2). The S peak is actually composed of two peaks, but the doublet is resolvable only in well-ordered CM (Vidano and Fischbach, 1978; Wang et al., 1989; compare Fig. 1a and 1b). The weak peaks at $\approx$3248 and $\approx$2450 cm^{-1} are observed in most samples of well-ordered graphite (Fig. 1a), but not in more disordered

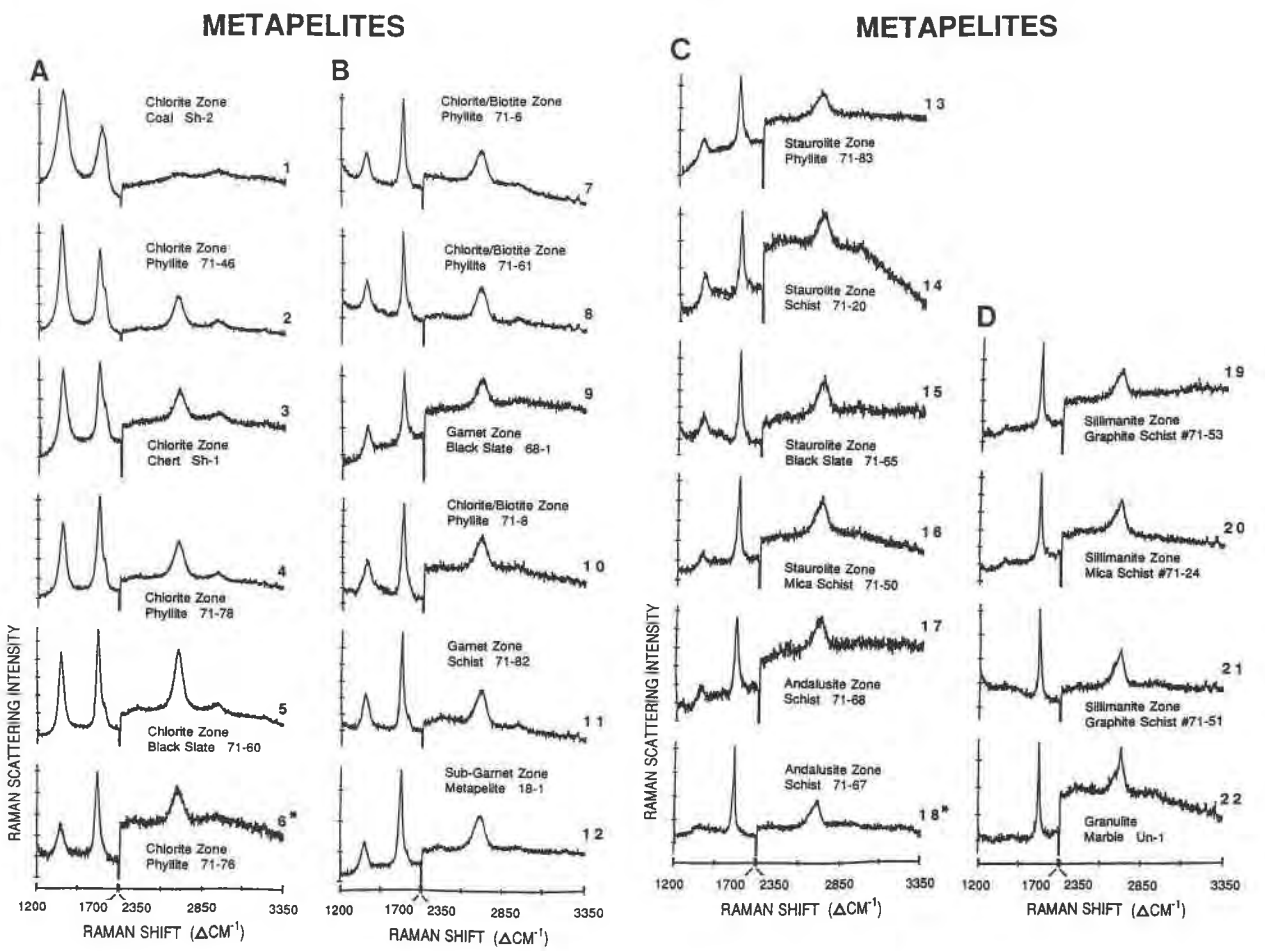

Fig. 2. Raman spectra of carbonaceous material hosted predominantly in metapelitic rocks. Location and rock types of all samples listed in Table 2. Four spectrally defined groups correlate with (**A**) chlorite zone, (**B**) biotite and garnet zones, (**C**) staurolite, kyanite, and andalusite zones, and (**D**) sillimanite zone and granulite facies. Two exceptional spectra marked with asterisks; see text.

forms of CM (Fig. 1b). In the latter, however, there is a wide low-intensity peak at $\approx$2940 cm^{-1} (see Figs. 1b and 2A) that may also be due to C-H stretching vibrations (Tsu et al., 1978). In general, we find that with decreasing crystallite size, the feature at $\approx$2735 cm^{-1} becomes broader, the one at $\approx$2940 cm^{-1} becomes more intense, and the peaks at $\approx$3248 and $\approx$2450 cm^{-1} become suppressed (compare Fig. 1a and 1b).

In summary, well-crystallized graphite shows the well-known first-order Raman peak at $\approx$1582 cm^{-1}, and four second-order peaks: a doublet at $\approx$2695 and $\approx$2735 cm^{-1} and two small peaks at $\approx$2450 and $\approx$3248 cm^{-1}. In more disordered forms of pure C, the latter two peaks become suppressed, and the others broaden; two new disorder-induced peaks appear at $\approx$1355 and $\approx$1620 cm^{-1}; and an additional peak is observed at $\approx$2940 cm^{-1}, which in natural CM may correspond to either the theoretically predicted disorder-induced band at $\approx$2950 cm^{-1}, or the C-H stretching vibration in impure CM.

Sample description and analytical technique

Samples

Raman microsampling spectroscopy was done on a total of 37 samples (Table 2) of carbonaceous materials, three of them artificially produced (nos. 26–28) and the rest naturally occurring. Of the natural samples, 24 are grain separates from various metamorphic terranes (nos. 2–23, 25, 30), eight are kerogen and coal grain separates (nos. 1, 31–37), and two are thin sections containing graphite (nos. 24, 29). With respect to the process of formation, only five samples (nos. 26–30) are examples of fluid-deposited CM (process 1, see above), whereas the CM in all other samples was transformed from organic precursors.

The 24 grain separates of graphite and coal (nos. 1–21, 23, 25, and 31) were generously provided by Edward S. Grew, from his 1974 study on carbonaceous materials.

TABLE 2. Raman spectroscopic parameters

Spectrum no.	Sample	Grade	Rock type	Locality	Peak pos D (Δcm^{-1})	Peak pos O (Δcm^{-1})	Peak pos S (Δcm^{-1})	Peak width D (cm^{-1})	Peak width O (cm^{-1})	D/O int. ratio	D/O area ratio	[D/(D + O)] × 100 by area	L_a (Å)
				Metapelites									
1	Sh-2	chlorite	shungite ("coal")	Shunga, Karelia	1350	1591	n.a.	76	70	1.49	1.94	66	4
2	71-46	chlorite	phyllite	Providence, RI	1348	1575	2694	42	39	1.26	1.27	56	21
3	Sh-1	chlorite	chert	Shunga, Karelia	1352	1577	2697	47	38	1.00	0.97	49	34
4	71-78	chlorite	phyllite	Austerlitz, NY	1352	1579	2702	43	33	0.74	0.97	49	34
5	71-60	chlorite	black slate	Portsmouth, RI	1351	1579	2700	37.5	29	0.79	0.86	46	43
6	71-76*	chlorite	phyllite	Mount Cube, VT quad.	1349	1570.5	2692	46	28	0.32	0.42	30	102
7	71-6	chlorite/biotite	phyllite	Peach Bottom, York Co., PA	1352	1581	2719	44.5	25	0.29	0.46	32	92
8	71-61	chlorite/biotite	phyllite	Portsmouth, RI	1353	1580	2715	40	22	0.34	0.59	37	70
9	68-1	garnet	black slate	Worcester, MA	1360.5	1585	2713	38	20	0.40	0.46	32	92
10	71-8	chlorite/biotite	phyllite	Peach Bottom, York Co., PA	1359	1581	2724	55	27	0.36	0.59	37	70
11	71-82	garnet	schist	Stockbridge, MA quad.	1352	1580	2727	47.5	22	0.35	0.65	39	60
12	18-1	subgarnet	metapelite	Bashbishfalls, MA-CT-NY quad.	1353	1577	2712	47.5	24	0.29	0.36	26	129
13	71-83	staurolite	phyllite	Stockbridge, MA quad.	1354	1570	2712	62	24.5	0.23	0.31	24	141
14	71-20	staurolite	schist	Worcester, MA	1354	1581	2731	47	22.5	0.29	0.56	36	84
15	71-65	staurolite	black slate	Jamestown, RI	1356.5	1580.5	2715	46	19	0.24	0.35	26	129
16	71-50	staurolite	mica schist	Jamestown, RI	1354	1578	2730	56	21.5	0.14	0.34	25	131
17	71-68	andalusite	schist	Ayer, MA quad.	1358	1571	2717	52	24	0.18	0.36	26	129
18	71-67*	andalusite	schist	Ayer, MA quad.	1356	1567	2706	79.5	16.5	0.09	0.21	17	339
19	71-53	sillimanite	graphite schist	South Kingston, RI	1357	1575	2715	68	17.5	0.09	0.21	17	339
20	71-24	sillimanite	mica	Boylston, MA	1353	1577.5	2709	49	18	0.09	0.12	11	786
21	71-51	sillimanite	graphite schist	South Kingston, RI	n.a.	1580	2723	n.a.	14	0.05	0	n.c.	n.c.
22	Un-1	granulite	marble	Sussex Co., NJ	n.a.	1580	2728	n.a.	13	0	0	0	∞

TABLE 2—*Continued*

Spectrum no.	Sample	Grade	Rock type	Locality	Peak pos D (Δcm^{-1})	Peak pos O (Δcm^{-1})	Peak pos S (Δcm^{-1})	Peak width D (cm^{-1})	Peak width O (cm^{-1})	D/O int. ratio	D/O area ratio	[D/(D + O)] × 100 by area	L_a (Å)
				Other rock types									
23	71-56	garnet	calcareous granofels	E. Greenwich, RI	1358.5 ± 1.0	1581.5 ± 1.0	2723.3 ± 3.6	48.0 ± 6.5	20.0 ± 1.7	0.22 ± 0.05	0.35 ± 0.05	26 ± 3	129 ± 23
					1358	1580.7	2718	57.5	18.0	0.17	0.36	26	129
					1360	1583	2724	44.0	22.0	0.18	0.29	22	164
					1358	1581	2725	44.5	19.5	0.27	0.36	26	129
					1358	1581.5	2726	45.0	19.9	0.24	0.40	29	109
24	CR4	garnet	tuffaceous metaflysch	Ketchikan, AK	1360	1578	2727	30	21	0.12	0.15	13	557
25	71-3	staurolite	marble	Towson, MD quad.	1353	1576.5	2723	63.5	17.5	0.09	0.17	15	429
				Fluids									
26	AA3	600 °C, 3 kbar	quartz	synthetic fluid inclusion	1330	1598	n.a.	106	48	0.55	1.03	51	30
27	IM740	740 °C, 2 kbar	powdery ppt.	synthetic	1351	1580	2723	39.5	23	0.31	0.57	36	84
28	602D	1400 °C, ≈5 kbar	mantle xenolith olivine	San Carlos, AZ; artific. re-equilibrated	1348	1581.5	2687	38.5	20	0.26	0.40	29	109
29	521	>600 °C, 1.5–2.0 kbar	hydr. altered troctolite	Duluth Complex, MN	n.a.	1581	2726	n.a.	16.5	0	0	0	∞
30	CEYL	granulite	vein graphite	Sri Lanka	1362	1578	2726	41	16	0.04	0.08	7	1643
				Kerogens									
31	Zen Coal	unknown	coal	unknown	1342	1600	n.a.	160	70	0.84	1.09	52	29
32	123-1-RK	"little or no" metam.	shale	McArthur Basin, N Terr., Australia	1355	1606	n.a.	153	74	0.71	1.28	56	21
33	114-1-RK	"little or no" metam.	shale	McArthur Basin, N Terr., Australia	1362	1600	n.a.	189	77	1.27	1.38	58	18
34	498-1-RK	subgreenschist	shale	Port Arthur Homocline, Ontario, Canada	1348	1607	n.a.	147	61	0.53	1.04	51	30
35	004-1-RK	lower greenschist	chert	Pilbara Block, W. Australia	1344	1597	n.a.	84	62	1.12	1.70	63	10
36	027-1-RK	pumpellyite-epidote	chert	Hamersley Basin, W. Australia	1344	1607	n.a.	84	47	0.74	1.43	59	16
37	198-1-RK	greenschist	chert	Onverwacht Gr., Barberton Greenstone Belt, S. Africa	1350	1600	n.a.	55	72	1.41	1.24	55	23

Note: All samples are grain separates with the following exceptions: 24 (thin section), 26 (polished wafer), 28 (polished wafer), and 29 (thin section). L_a, in-plane crystallite dimension (in ångströms), is determined from average correlation curve (as shown in Figs. 10 and 11), based on calibration results from Tuinstra and Koenig (1970a) and Beny-Bassez and Rouzaud (1985); n.a. = not applicable; n.c. = not calculable.

* Unusual samples; see text.

Some Raman results on sample nos. 1–21 were previously reported in Pasteris and Wopenka (1991), in which the exact origin of those samples is described (see also our Table 2). Additional geologic information concerning the origin of Grew's sample is given in Thompson and Norton (1968), Grew and Day (1972), Rumble et al. (1977), Zen (1981), Wintsch et al. (1981), Murray (1987), and Mosher et al. (1987). Two other samples in Grew's suite that require some further explanation are the shungite (a coal-like material, no. 1) and Shung chert (no. 3) from Karelia. The latter two samples were found close to each other, one in a coal-rich and the other in a more cherty facies (Grew, personal communication, 1989). Another coal sample (no. 31), whose documentation is no longer available, was provided by E-an Zen for Grew's (1974) study. Of importance here is the fact that most of those samples have similar rock types (metapelites) but differ in their original precursor chemistry (e.g., both marine and nonmarine sediments are represented), and also have experienced various types of metamorphism. For instance, eight samples (nos. 2, 5, 8, 15, 16, 19, 21, and 23) underwent Barrovian-type metamorphism, whereas three other samples (nos. 11–13) experienced two major episodes of metamorphism during Taconian (Ordovician) and Acadian (Devonian) orogenies.

Grew (1974) provided the following data on his grain separates: particle size, bulk content of C, H, N, and O, width and position of the (002) peak derived by XRD of bulk grain separates, and mineralogy and metamorphic grade of the host rock. Identification of metamorphic grade was provided by Grew (personal communication) for those metapelites that are not documented in his 1974 paper. Grew (1974) gave a detailed description of the extraction of CM from its rock matrix through crushing and acid dissolution. Care was taken not to change the chemistry or crystal structure of the material. Some of Grew's samples (nos. 1–3, 9, 10, 15, 19, and 23) also were studied by HRTEM by Buseck and Huang (1985).

Six grain separates of Precambrian kerogens (nos. 32–37) were provided by John Hayes and Harald Strauss (Hayes et al., 1983; Wedeking and Hayes, 1983). Buseck et al. (1988) subsequently did an HRTEM study on the kerogens that had been documented by Hayes et al. (1983), including four (nos. 32–34, 36) of the six kerogen samples that we analyzed by LRM spectroscopy.

The remaining four natural samples are CM within doubly polished thin sections (no. 24 and no. 29) or in the form of well-crystallized graphite flakes (no. 30 and no. 32). Sample no. 30 is a visually homogeneous sample of vein-type Sri Lankan graphite, 40 × 10 cm (exact locality not specified), from the economic geology collection at Washington University. Sample no. 22 is of Precambrian Franklin marble with disseminated graphite flakes from Sussex County, New Jersey, collected in the Limecrest quarry by J.D.P. A thin section provided by Maria Luisa Crawford (no. 24) consists of graphite platelets in a tuffaceous metaflysch from the Gravina Belt on the Cleveland Peninsula in the western part of the Ketchikan Quadrangle, Alaska. The other thin section (no. 29) consists of bladed graphite spherulites (about 1 mm in diameter) in hydrously altered troctolite from the base of the Duluth Complex in Minnesota (from drill core provided by Henk Dahlberg; thin section loaned by David C. Sassani). The graphite blades that were analyzed are embedded in quartz (see Pasteris, 1989).

For comparison with the natural samples, three types of synthetically precipitated CM also were analyzed. The first sample (no. 26) is embedded in a doubly polished wafer of pure Brazilian quartz in which C-O-H fluid inclusions were synthetically produced by S. Michael Sterner and Robert J. Bodnar (Sterner and Bodnar, 1984) using a mixture of acetic acid and H_2O taken to 600 °C and 3 kbar in a closed hydrothermal system. The CO_2-CH_4-H_2O fluid inclusions, in which the CM precipitated, were previously analyzed by microthermometry and Raman microsampling spectroscopy (Seitz et al., 1987). The second sample (no. 27) is CM powder that was deposited from a CH_4-H_2 mixture in a closed furnace at 740 °C and 2 kbar in an experiment by I-Ming Chou (see Chou, 1987). The third sample (no. 28) is a CM coating on an originally pure CO_2 fluid inclusion in an olivine grain in a mantle xenolith from the San Carlos volcanic field in Arizona. CM was artificially induced to precipitate in the inclusion during an experiment by B. J. Wanamaker at 1400 °C and log $f_{O_2} = -10$, an f_{O_2} about equivalent to that of the Fe + wüstite buffer. This sample is a doubly polished wafer; the inclusion is several micrometers in diameter (Pasteris and Wanamaker, 1988).

Raman analysis

Raman microsampling spectroscopy was done using a 1983 model Ramanor U-1000 (Instruments SA) LRM with an Olympus BH2-based microsampling accessory. Additional details of the instrument and analytical procedures are reported in Pasteris et al. (1988). The microscope objective used is a 40× Nachet with a numerical aperture of 0.75. Irradiation was by the 514.5-nm line (=19435 absolute cm^{-1}) of a continuous-wave Ar-ion laser (Coherent Innova 90-5). Because of the high extinction coefficient of carbonaceous material for the laser beam, the Raman spectrum originates from a relatively thin surface layer of the sample (usually <1000 Å). Depending on how stable the CM remained during analysis, the laser intensity was varied between 1 and 15 mW at the sample surface. Each sample was scanned from 1200 to 1700 relative cm^{-1} (Δcm^{-1}) for the first-order Raman spectrum and from 2350 to 3350 Δcm^{-1} for the second-order Raman spectrum at a spectral resolution of about 5 cm^{-1}. [Note that the frequencies of the signals recorded (Raman shifts in Δcm^{-1}) are relative to the frequency of the exciting light, and thus the actual wavelengths measured are in the visible part of the electromagnetic spectrum.] Photon detection was by single-channel analysis, with an RCA C31034-2 photomultiplier tube that was thermoelectrically cooled to −30 °C. The stepping interval was 1 cm^{-1}, and the dwell time was 10 s per point,

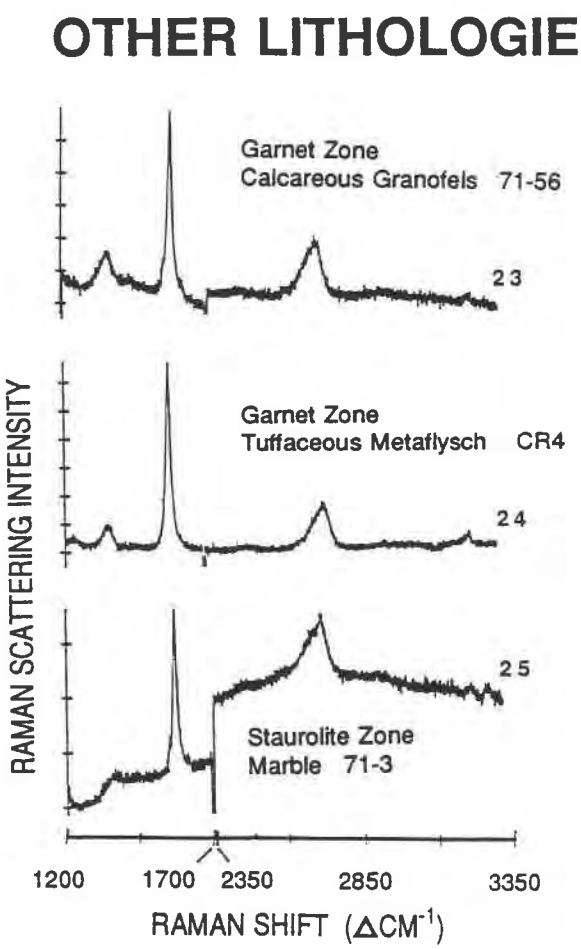

Fig. 3. Raman spectra of carbonaceous material hosted in nonpelitic rocks. Refer to text and Table 2 for exact location and description of samples. Comparison of Figs. 2 and 3 shows that under similar *P-T* conditions graphitization proceeds to different degrees in rocks of different rock types.

totaling 4.5 h minimum analysis time for one sample. In numerous cases, up to four scans taken under the above analytical conditions had to be summed to obtain a satisfactory signal to noise ratio, as shown in Figures 1–5. Spectra with a comparable signal to noise ratio can be obtained in a matter of minutes using a multichannel detector and a triple-monochromator system (unpublished data).

Sample preparation

The major concerns about sample handling for CM involve sample stability under the laser beam and spectral artifacts caused by grain orientation and the effects of polishing and mechanical separation. Much of the laser-induced heating of the opaque CM was eliminated by pressing samples available in form of grain separates (i.e., all samples except nos. 24, 28, and 29) into Au foil, which acted as a heat sink. First, a standard Al stub, 12.7 mm O.D., as is used for SEM and ion-microprobe work, was finely scribed on its upper surface. Then, a specially de-

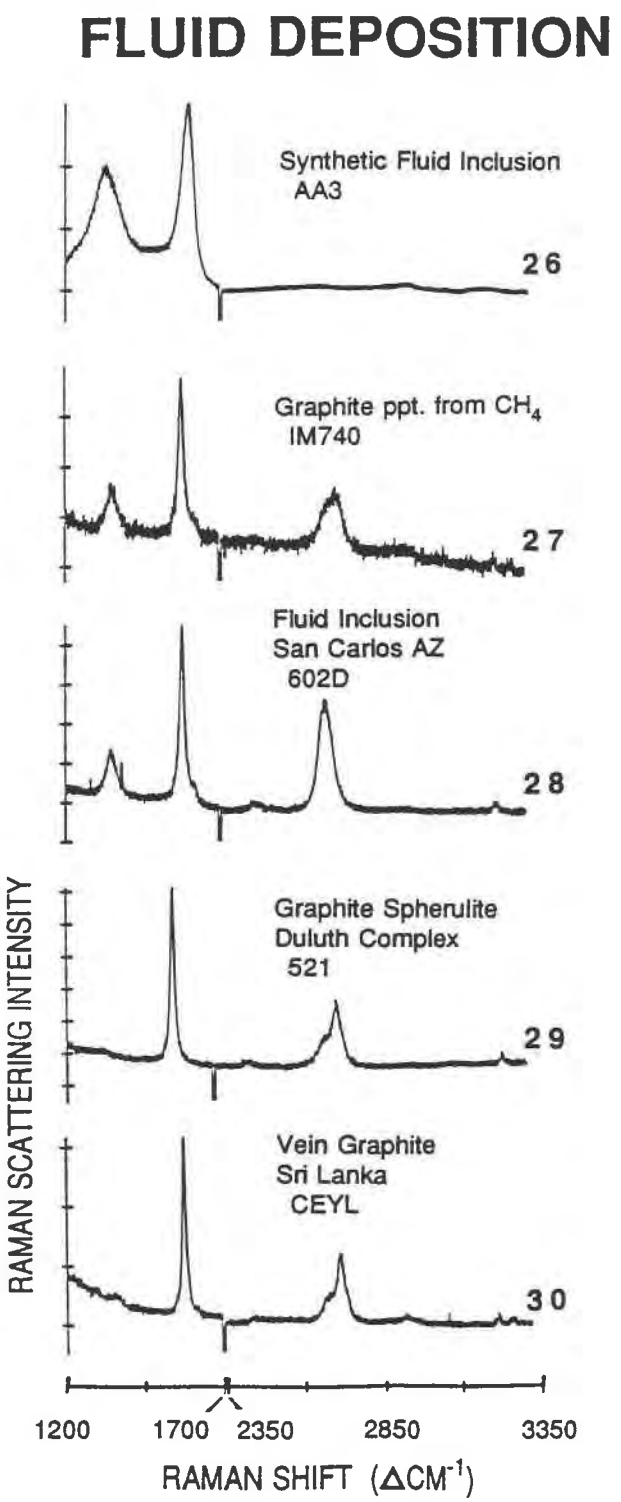

Fig. 4. Raman spectra of carbonaceous material known or inferred to have been deposited from fluids. Refer to text and Table 2 for description of samples.

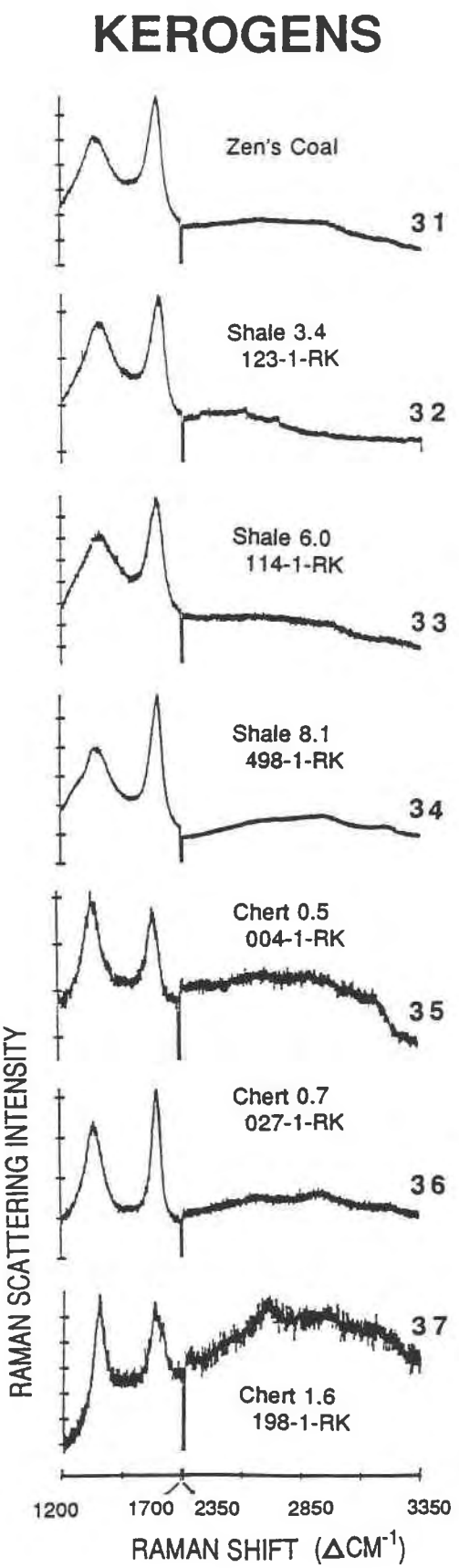

signed press was used to fix a square of Au foil approximately 5 × 5 mm (≈12 μm thick) onto the stub; cold flow of the Au into the irregularly scribed furrows on the stub seals the Au onto the stub's surface. The Au subsequently was sputtered in an ion mill to remove any contaminants from its surface. In a clean-lab environment, a commercially available micromanipulator was used to place CM particles onto the Au foil. Another specially designed press was used to carefully embed the CM grains in the Au foil by means of pressure from a glass plate, while their position was monitored under a microscope; this technique had been developed for pressing individual interplanetary dust and small meteorite grains into Au for SEM and ion-microprobe analysis. In many cases, operation at the usual 15-mW laser power at the sample surface still was not possible, but reduction in laser intensity permitted adequate to excellent Raman spectroscopic analysis of all but one (not included in Table 2) of the CM samples subject to this study. In general, the more disordered the CM, the more likely it is to be unstable in the laser beam. A combined secondary ion mass spectrometry and LRM study of interstellar CM also revealed a correlation between high H^-/C^- and CN^-/C^- ratios (indicating high content of atoms other than C) and sensitivity to the laser beam (Zinner et al., 1990). Several samples were analyzed by LRM in situ in polished wafers or thin sections, which also act as a heat sink for the graphite grains. Our experience is that graphite grains analyzed in situ generally give a better Raman spectrum (a higher signal to noise ratio) than similar grains laid on a glass slide or even pressed into a Au mount. Part of this spectral quality is due to better heat removal (compared with resting on a glass slide), but some of it probably is due to optical effects created by the overlying matrix mineral.

The effect on the recorded Raman spectrum of grain orientation with respect to the plane of polarization of the laser beam has been addressed in the Raman literature only recently (e.g., Katagiri et al., 1988; Pasteris, 1989; Wang et al., 1989). The intensity ratio (i.e., the peak-height ratio) $I_{\approx 1355\ cm^{-1}}/I_{\approx 1600\ cm^{-1}}$ depends on both the degree of graphitization and the scattering geometry, i.e., the orientation of the graphitic planes with respect to the polarization orientation of the exciting laser beam. If one of the parameters can be assumed to be constant, the other can be compared between samples. Since the surface of highly crystalline CM is usually defined by basal planes, most of the earlier Raman work on graphite was conducted on basal sections, and little attention was paid to orientation. The pressing of graphite grains into Au mounts seems to enhance the preferred orientation of the

←

Fig. 5. Raman spectra of kerogens and coal. Refer to text and Table 2 for description of samples. Numbers above sample name represent total organic C (milligrams of C per gram of rock).

grains, with the basal planes parallel to the mount (perpendicular to the laser beam), compared with their orientation as loose grains on a glass plate. However, the effects of orientation on the Raman spectra of CM require that caution be exercised in the interpretation of the Raman spectra of microcrystalline ("disordered") forms of graphite precipitates, such as those on the walls of fluid inclusions.

The question of polishing and other mechanical effects also has been discussed before (Nakamizo et al., 1978; Nemanich and Solin, 1979; Beny-Bassez and Rouzaud, 1985; Katagiri et al., 1988; Pasteris, 1989; Wang et al., 1989). Experiments indicate that prolonged polishing of the sample surface can cause severe disorder effects in the spectrum. Nakamizo et al. (1978) showed by means of Raman spectroscopy that the crystal structure of graphite is gradually destroyed with increasing grinding time. Their results indicate that the structural defects introduced into natural graphite during the grinding process are different from those that are originally present in synthetic coke, which are gradually removed during the graphitization process. On the other hand, we have analyzed graphite grains released from their matrices by ball milling (in other studies) and have found their Raman spectra to be indistinguishable from those for granulite-grade graphite. Nevertheless, the best procedure is to avoid mechanical disruption of the sample. In terms of in situ LRM analysis in polished thin sections or wafers, one should focus the laser onto a properly oriented graphite grain beneath the surface of an adjacent transparent grain, such as quartz (Pasteris, 1989). Such graphite grains are left unaffected by surface polishing. It should be noted that the requirement of careful sample handling of graphite is not peculiar to Raman analysis; it is also essential for XRD and HRTEM analysis.

Results and discussion

Raman spectral data

The main spectral results of this study are displayed in the spectra in Figures 2–5 and listed in Table 2. The peak width was measured as full width at half maximum (FWHM); the background and integration limits for peak area calculations were determined visually for each individual spectrum and varied slightly among different spectra; and the peak position was determined at maximum intensity. (The alternative approach of locating the peak position by determining the peak center at the half maximum was not applied to CM samples because of the occurrence of extremely broad peaks and irregular peaks representing band overlaps.)

Figure 2 shows the close correlation between the Raman spectral features and the grade of metamorphism of carbonaceous material in a suite of rocks with similar rock types (all pelites except for nos. 1, 3, and 22), but a range of types of initial organic matter. [The spectra no. 1 and no. 3 (Shungite coal and Shung chert from the chlorite zone) and no. 22 (granulite-facies graphite hosted in a marble) are included in Figure 2 for completeness of the metamorphic sequence shown.] The CM samples in Figure 3 are hosted by various other nonpelites. Figure 4 shows spectra of both natural and artificial CM that are known or inferred to have been deposited from fluids, whereas the spectra of kerogens and another coal are shown in Figure 5. These four figures demonstrate that the Raman spectrum of CM is sensitive to changes in the degree of ordering in materials ranging from kerogens and coal to granulite-facies, coarsely crystalline graphite.

The visual ordering of the spectra from the C-bearing metapelites (Fig. 2), interpreted according to the discussion above and as in the cited references concerning order-disorder relations, agrees with the metamorphic grouping of the samples (with the exception of the two samples mentioned below). The visual ordering also shows that there are several breaks in the development of the major spectral features: the spectra cluster into four subdivisions, as shown in columns A through D in Figure 2. The four spectral groups are defined geologically as follows: (A) chlorite zone, (B) biotite and garnet zones, (C) staurolite, kyanite, and andalusite zones, and (D) sillimanite zone and granulite facies. These four groups will be referred to as metamorphic categories. The two spectra marked with an asterisk in Figure 2 (sample 71-76* in column A and sample 71-67* in column C) have been placed according to their reported metamorphic mineral assemblages (chlorite zone and andalusite zone, respectively; Grew's samples, documented in Buseck and Huang, 1985), and the mapped isograds of Thompson and Norton (1968). In both cases, however, their Raman spectral features would place these samples at the beginning of the next higher grade metamorphic category. (Unfortunately, no XRD or HRTEM data are reported on these two samples in the studies of Grew, 1974, and Buseck and Huang, 1985, respectively.)

In order to check the significance of the sequencing of the spectra in Figure 2, tests were performed for both reproducibility (repeated analyses of the same sample spot) and heterogeneity (analyses of several different grains from one sample). Whereas the reproducibility of peak positions, widths, and intensities of Raman peaks was tested only for one sample (71-56, see Table 2), heterogeneity was tested for most samples. Typically, the degree of parameter variation that was monitored in the heterogeneity test was only slightly greater than that for the reproducibility test, indicating the homogeneity of the samples. The major exception is the black slate 71-60 from the chlorite zone (Fig. 2A, spectrum no. 5), some of whose spectra indicate higher degrees of metamorphism (see discussion below).

The grade of metamorphism and degree of graphite crystallinity increase downward in each column (metamorphic category) in Figure 2 (see also Table 2). Category A, representing the lowest grade of metamorphism, shows the greatest range of features in both the first- and second-order spectra. The second-order spectrum of coal (Shungite Sh-2) looks very different from that of the other CM

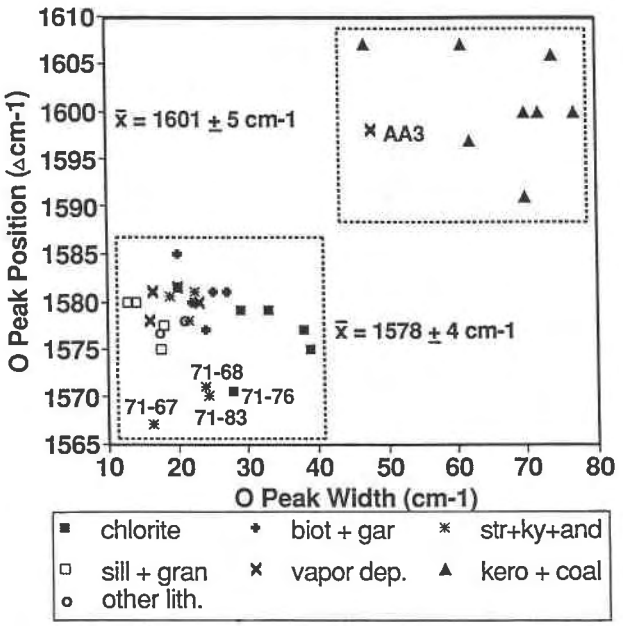

Fig. 6. Peak position vs. peak width (FWHM) of O peak. Graph includes all samples from Table 2. Symbols refer to different sets of samples, as defined in text. Samples define two groups, as indicated by dashed lines. Average values and 1σ errors for O peak positions are calculated for samples 1, 26, 31–37, and all other samples. Four samples with anomalously low O peak positions are labeled.

in the chlorite zone. The breadth of its first-order peaks and the almost total absence of second-order spectral features instead resemble the kerogen spectra and another coal spectrum (Fig. 5) discussed below. Coal sample Sh-2, as well as the unusual sample 71-76*, will both be excluded in the following discussion concerning spectra in column A. In the progression from most to least disordered CM (from top to bottom of column A), the D : O intensity ratio decreases in the first-order spectrum from 1.26 to 0.74, with a mean (n = 4) of 0.95 ± 0.2. In most samples, a low-intensity shoulder is resolved on the high-wavenumber side of the O peak. The band shapes of the second-order spectra look similar among the samples despite the large change in D : O. The main second-order peak (S peak) is symmetric; i.e., the doublet cannot be resolved, and its position of maximum intensity is unusually low compared with the theoretically expected position of ≈2735 cm^{-1} [mean for chlorite grade samples (n = 4) is 2698 ± 4 cm^{-1}]. The peak at ≈2940 cm^{-1} is clearly present in all but the unusual sample 71-76*. The average width (FWHM) of the O peak is 35 ± 5 cm^{-1} for spectra in column A (unusual samples Sh-2 and 71-76* not included).

There is a definitive break (again, with the exception of sample 71-76*) in spectral features between samples from the chlorite zone (column A) and those from the chlorite-biotite and garnet zones (column B). This discontinuity is especially evident in the sharp change in the D : O intensity ratio, ranging from 0.40 to 0.29 [mean (n = 6) of 0.34 ± 0.04] for column B spectra. In contrast to the wide spectral variations shown in column A, the spectra in column B are quite similar. In those spectra, the peak at ≈2940 cm^{-1} is weaker than in column A, in accord with the identification of this band either as disorder-induced or reflecting C-H stretching. The S peak is significantly shifted to higher wavenumbers [mean (n = 6) position for column B spectra is 2718 ± 6 cm^{-1}] compared with spectra in column A but remains symmetric, i.e., unresolved. Three of the spectra in column B (nos. 7, 8, and 11) show two small peaks, ≈3240 and ≈3300 cm^{-1}, whereas only one high-wavenumber second-order peak at ≈3248 cm^{-1} is predicted theoretically (e.g., Elman et al., 1981). The latter peaks are not obvious in most spectra of column C, but they do appear in higher grade samples (column D), as well as in most fluid-deposited CM (Fig. 4), and in samples of nonpelitic rock type (Fig. 3). The origin of the small peak at ≈3300 cm^{-1} remains unexplained to date but is believed not to be an artifact. (There is a peak at 3327 cm^{-1}, apparently induced by the coating on the 40× microscope objective. However, the latter was seen only when the laser light was scattered by a polished Au substrate and was not detected in our Raman spectra of CM.) The average width of the O peak is 23 ± 3 cm^{-1} for spectra in column B. As for most spectra in column A, there is a small shoulder on the high-wavenumber side of the O peak (a shoulder on the low-wavenumber side of the O peak, as seen, e.g., in spectrum no. 11, arises from O_2 in the air at 1555 cm^{-1}).

The spectra of samples from the staurolite and andalusite zones (category C) are distinguished from those in column B by their lower D : O intensity ratios and especially by the asymmetry of the S peak, even though its spectral components remain unresolved. The D : O intensity ratios range from 0.29 to 0.14 with a mean (n = 5) of 0.22 ± 0.06. (The exceptional sample 71-67* has a D : O of 0.09 and is not included in the mean.) The average O peak width for column C spectra, excluding sample 71-67*, is 22 ± 2 cm^{-1}. A small disorder-induced high-wavenumber shoulder remains on the O peak (in addition to the O_2 artifact on the low-wavenumber side) in all but the most ordered graphite in this category. In the progression from lowest to highest degree of ordering of the CM (top to bottom of Fig. 2C), the S peak becomes progressively more asymmetric.

The spectra of samples from the sillimanite zone and granulite facies (category D) are distinguished from those in column C by the (almost) total disappearance of the D peak in the first-order spectrum. The D : O intensity ratios range from 0.09 to zero, and the average O peak width (n = 4) is 16 ± 2 cm^{-1}. In the progression from lowest to highest degree of ordering of CM (top to bottom in Fig. 2D), the S peak becomes increasingly more asymmetric, reflecting its two spectral components.

In summary, the decrease in both the D : O intensity ratios and the O peak widths are relatively sensitive mea-

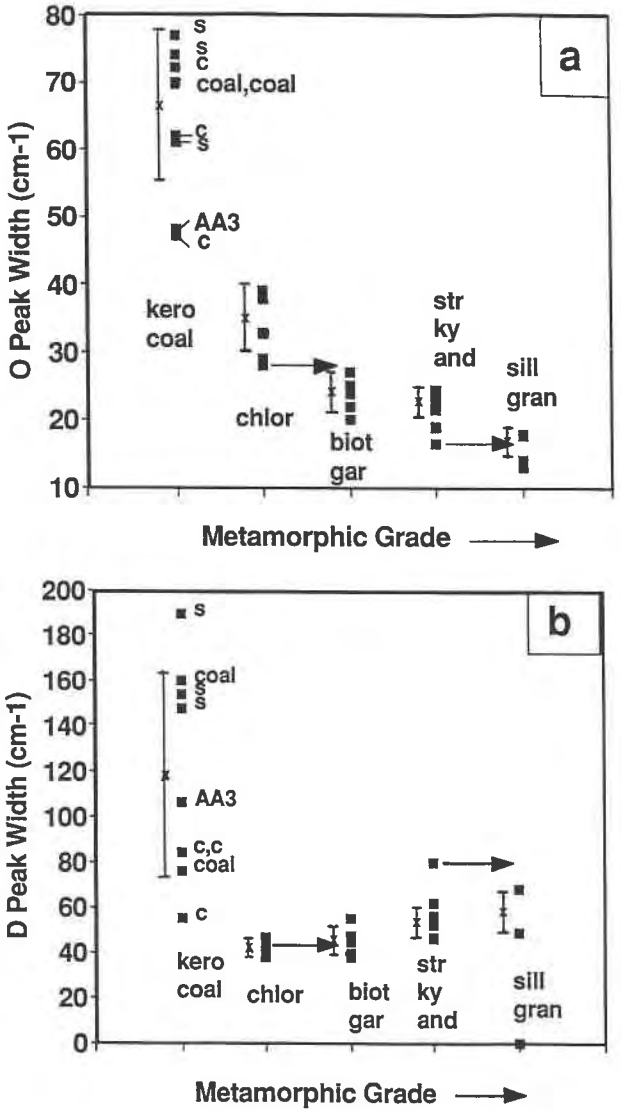

Fig. 7. (a) Peak width (FWHM) of O peak vs. metamorphic category; (b) peak width (FWHM) of D peak vs. metamorphic category. Graphs a and b include samples 1–22, 26, and 31–37. Shale-hosted (S) and chert-hosted (C) kerogens as well as coals and sample AA3 are labeled. Average values and 1σ errors are shown for each metamorphic category. Unusual samples 61-67* and 61-76* are not included in calculation; arrowheads indicate the metamorphic categories to which those two samples are believed to belong (see text).

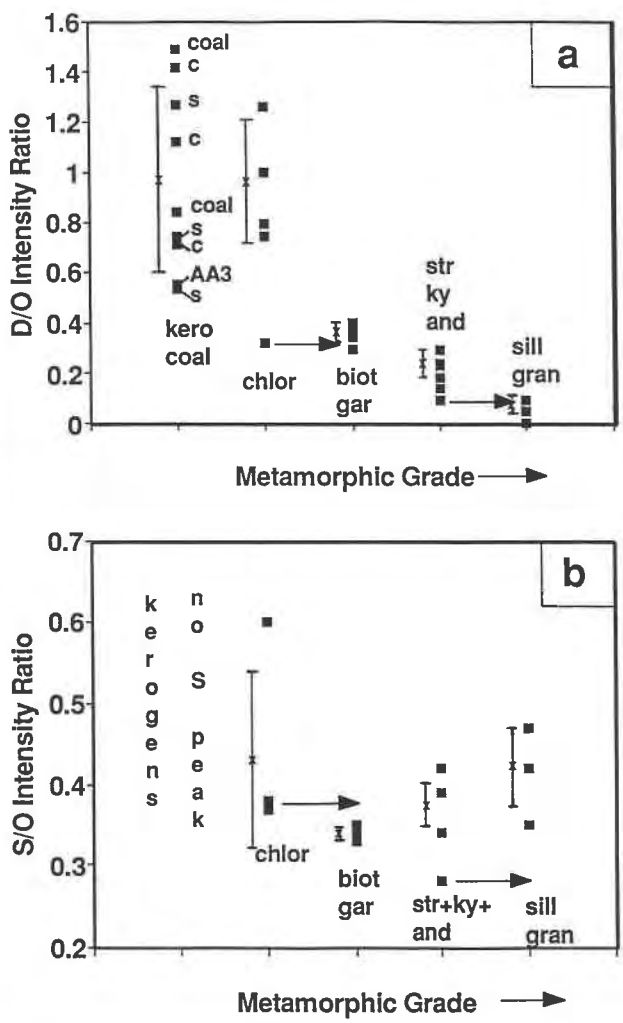

Fig. 8. (a) Intensity ratio of D peak to O peak vs. metamorphic category; (b) intensity ratio of S peak to O peak vs. metamorphic category. Graphs a and b include samples 1–22, 26, and 31–37. Shale-hosted (S) and chert-hosted (C) kerogens, coals, and sample AA3 are labeled. Average values and 1σ errors are shown for each metamorphic category. Unusual samples 61-67* and 61-76* are not included in calculation; arrowheads indicate the metamorphic categories to which these two samples are believed to belong (see text).

sures of the increase in degree of crystallinity and grade of metamorphism of CM (Figs. 6, 7a, and 8a, Table 2; see also Fig. 4 in Pasteris and Wopenka, 1991). A break is recognized between metamorphic categories A and B at the stage at which the O and D peaks cease to be subequal in maximum intensity (exception: no. 71-76*). However, the D : O intensity ratio continues to be the best spectral parameter for recognizing progressive changes in metamorphism and crystallinity in category B, and it is still a useful indicator of metamorphic grade in category C. The transition between categories B and C is recognized by the development of asymmetry in the S peak, which is progressively resolved into its two components. Samples from the sillimanite zone and granulite facies (metamorphic category D) are recognized by the (almost complete) absence of a D band in the first-order spectrum.

Figure 3 shows the Raman spectra of three graphitic samples whose host rocks are nonpelites. The calcareous granofels 71-56 is the only nonpelitic sample from Grew's (1974) suite of New England rocks, and the marble 71-3 is one of his samples of the Cockeysville marble in Maryland. Granofels 71-56 was collected from the garnet zone

but has a Raman spectrum that, by comparison with Figure 2C, would place it in the staurolite zone. Marble 71-3 is from an area mapped as part of the staurolite zone (zone boundaries not well defined in portions of this region), but the spectrum resembles those in Figure 2D from the bottom of the sillimanite zone. The mineral assemblage of sample CR4, a metaflysch, places it at the bottom of the garnet zone (M. L. Crawford, personal communication). However, its overall Raman spectrum resembles those for staurolite-zone metapelites (see Fig. 2C).

Figure 4 shows the Raman spectra of CM that are known or inferred to have been deposited from fluids. These samples represent a wide range of depositional histories, rock types, and sampling geometries (blades embedded in rock wafers, coatings on fluid inclusions, pressed powders, grains lying on glass), and thus provide a test of the general applicability of the spectral observations derived for the samples discussed above. The graphite spherulite sample hosted in a troctolite in a thin section (521) and the grain mount from Sri Lankan vein graphite (CEYL) have first-order spectra that are almost indistinguishable from that for CM extracted from a granulite-facies marble (see sample Un-1 in Fig. 2D). The major difference is the higher signal to noise ratio in the second-order spectra for 521 and CEYL than in that for Un-1. The values for the D : O intensity ratio and the O peak width also would place the latter two samples in the sillimanite-zone and granulite-facies categories, as defined above. The spectra for both the inclusion-coating CM hosted by olivine in sample 602D and the grain mount of methane-precipitated powder in IM740 resemble those for metapelites from the lower staurolite or higher biotite-garnet zones. The marked difference is that the intensity ratio of the S and O peaks ($I_{\approx 2700\ cm^{-1}}/I_{\approx 1600\ cm^{-1}}$) is much greater in the spectrum for 602D than in any other spectra with comparable D : O intensity ratios. This spectral relationship appears to be characteristic of the graphite coatings on inclusion walls in this sample (see also Pasteris et al., 1988, their Fig. 2A on p. 982; Pasteris and Wanamaker, 1988, their Fig. 2B on p. 1080). We have observed the same high $I_{\approx 2700\ cm^{-1}}/I_{\approx 1600\ cm^{-1}}$ ratio in a quartz-hosted CO_2-inclusion in which graphite was artificially induced to precipitate (Morgan et al., 1993). A comparison of the Raman spectrum for AA3, which is a CM precipitate in an artificially produced fluid inclusion hosted in quartz, with those of other CM samples discussed above that have comparable D : O intensity ratios shows several important differences: (1) the D peak in AA3 is anomalously broad, (2) the O peak is broad but has no shoulder, and (3) the second-order peaks are essentially absent. In these three regards, the spectrum for sample AA3 bears a much stronger resemblance to those shown in Figure 5 for kerogens and to those in Figures 2A and 5 for coals than to the ones for metapelites and other graphitic CM. Given the well-formed appearance of the graphite granules in sample AA3, their spectral immaturity is surprising.

Figure 5 shows the Raman spectra for six Precambrian kerogen samples and one coal sample. The samples of kerogens and coals (see also Fig. 2A, spectrum no. 1) are thermally less mature than all the other studied forms of CM [both fluid-deposited (with the exception of AA3), and derived from various organic precursors], and thus have Raman spectral properties grossly different from the latter. Kerogens and coals have (1) no (or very weak) second-order Raman features, (2) O peak positions shifted to higher wavenumbers compared with other CM (Fig. 6), and (3) very wide first-order peaks. They lack the 2940-cm^{-1} peak observed in many of the less mature metapelite-hosted CM, bringing into question the assignment of this peak to C-H stretching. The fluid-deposited sample AA3 (spectrum no. 26) resembles the kerogens and coals in all of the above aspects. A well-recognized cause for an upward shift in the O peak in CM is a change in peak shape caused by the development of a band (a high-wavenumber shoulder) at $\approx 1620\ cm^{-1}$, which reflects disordering. At very high degrees of disorder, the shoulder on the O peak cannot be resolved, leading to eventual broadening and effective upward shift of the O peak in highly disordered CM, as seen in the kerogen, coal, and AA3 samples from this work.

The kerogen spectra define two groups: the bottom three spectra in Figure 5 have narrower first-order peaks and stronger second-order features than the top three kerogen spectra. It is on this basis that the former have been interpreted as more mature than the latter, an interpretation that is in agreement with their assigned metamorphic grades (Hayes et al., 1983; see our Table 2). Thus, for kerogens, both the D : O intensity and area ratios are less reliable than measurements of peak widths for the interpretation of metamorphic grade, in distinction to the metapelite spectra. Another interesting observation is that the division of the kerogens into two spectral groups coincides with the distinctions between the high-C and the low-C samples (total organic C in bulk rocks; see numbers in Fig. 5) and between the shale-hosted and the chert-hosted kerogens, respectively. The spectrum of Zen's coal (no. 31) is very similar to the spectra of shale-hosted kerogen, whereas the other coal spectrum (no. 1) strongly resembles the chert-hosted kerogen spectra. We therefore conclude that Zen's coal is less mature, even though the information on locale and metamorphic grade for this sample has been lost. The present set of kerogen samples does not permit an evaluation of whether it is the rock type or the metamorphic grade (or both?) that controls the degree of crystallinity. Given the complexity of kerogen chemistry and genesis (e.g., Tissot and Welte, 1984), it is not possible to give a definitive interpretation of these data until more work is done on additional kerogen samples.

Quantification of Raman spectra of carbonaceous materials

Given the above correlations between the thermal history of a sample and its Raman spectrum, the question

arises if there are one or more measurable spectral parameters that (through calibration or calculation) can yield quantitative structural information on graphite. Our conclusions about and approaches to the quantification of Raman spectroscopy of CM differ from those of Haaland et al. (1990). The latter investigated only the D and O peaks, which they found pertinent for estimating the maximum temperature (375–2700 °C) experienced by C phenolic heat shields. However, our measured heights, areas, widths, and positions of the peaks in all the Raman spectra recorded (Table 2) indicate that single parameters are not as definitive as the covariation of various parameters, as discussed below (see also Pasteris and Wopenka, 1991).

The data on peak positions for the O band are of particular interest in CM. A comparison of the literature data on highly ordered, single-crystal graphite shows a wide range of reported values for this peak position (in cm^{-1}): 1575 (Tuinstra and Koenig, 1970a), 1580 (Vidano and Fischbach, 1978; Lespade et al., 1982), 1581 (Nemanich and Solin, 1979), and 1586 (Tsu et al., 1978). As shown in Table 2 and Figure 6, the recorded O peak positions of the CM from the graphitic samples (i.e., all samples excluding the coals, kerogens, and AA3) range from 1567 to 1585 cm^{-1}. There is a poor correlation between metamorphic grade and O peak position, especially in samples from the staurolite and andalusite zones. Three of the latter (samples 71-83, 71-68, and 71-67*) were found to have anomalously low O peak positions (see Table 2, Fig. 6). HRTEM studies were performed by Thomas Bernatowicz (Departments of Physics and Earth and Planetary Sciences at Washington University) on andalusite sample 71-67* in order to investigate structural and compositional features that could account for its anomalously low Raman O peak position (1567 cm^{-1}). Lattice-fringe images, electron diffraction patterns, and calculated *d* values showed nothing but perfectly normal well-crystallized graphite. Thus, the low O peak position in sample 71-67* remains unexplained to date.

We previously had recorded an unexplained low O peak position of 1565 cm^{-1} in very well ordered (no D-peak) graphite from a highly metamorphosed marble in Ontario (Wopenka et al., 1988; Wopenka and Pasteris, 1988). We also have documented similar downward shift of the O peak in highly crystalline graphite from mantle xenoliths (Pearson et al., 1991) and in interstellar graphite grains extracted from the Murchison meteorite (Zinner et al., 1990). Several authors have addressed the narrowing and downward spectral shift of the O peak in Raman spectra of progressively heat-treated CM. Chieu et al. (1982) showed smooth-curve relationships between heat-treatment temperature and (1) position of the O peak (lowest: 1580 cm^{-1}), (2) widths of the D and O peaks, and (3) D : O intensity ratio. Wang et al. (1989) reported a smooth-curve relationship between decrease in O peak width and decrease in O peak position from about 1581 to 1576 cm^{-1} for graphite associated with progressively altered rocks in an aureole around a U deposit. The graphite grains from the latter study show optical evidence of progressive pitting and structural disruption with decreasing distance to the deposit. Such Raman studies on the progressive heat treatment and radioactive exposure of a single type of CM clearly are better tests of the relationship between peak position and degree of crystallinity than is this study, in which many variables are uncontrolled. More work is required to clarify the controls on the O peak position, which potentially could provide important structural information about a sample.

There is a considerable range in values of O peak widths within each metamorphic category, with a significant overlap for samples of the biotite through andalusite zones (Fig. 7a). However, the average O peak widths of the metamorphic categories are distinguishable, with the exception of the categories biotite + garnet, and staurolite + kyanite + andalusite. Of note is the particular distinctiveness of the kerogen and coal samples, as well as of samples from the chlorite zone: from their O peak widths, each individual sample can be recognized as belonging in its proper category. Even though the O peak width for samples from the chlorite zone through granulite facies is correlated with the degree of crystallinity of CM, the same is not that obvious for either their D peak width (Fig. 7b) or D peak position (not shown). In this respect, our results differ from those of Chieu et al. (1982) and Beny-Bassez and Rouzaud (1985), who found the D peak width to be correlated with the degree of crystallinity in their progressively heat-treated synthetic CM. We found the latter correlation to be true only for our kerogen and coal samples. Indeed, it is the D peak width or a combination of the D peak width and the D : O area ratio that are the only indicators of maturity in CM samples not sufficiently well crystallized to have a well-developed second-order spectrum. Neither the D : O area ratio nor the D : O intensity ratio is an accurate indicator of the in-plane crystallite size for those kinds of materials. (The usefulness of the D : O area ratio is difficult to evaluate from our data, however, because the chosen spectral windows do not allow an accurate determination of peak areas, given the extremely wide first-order peaks of kerogens and coals.) For better-ordered CM (i.e., graphitic material), the more easily measured D : O intensity ratio is an informative indicator of metamorphic grade. As Figures 7a and 8a illustrate, for most of the C-bearing metapelites in this study, the different metamorphic categories can be distinguished according to their O peak widths and D : O intensity ratios. Because of their much higher D : O intensity ratios, the chlorite-zone samples are very easily distinguished from higher grade samples (Fig. 8a). There is some overlap in D : O intensity ratios of individual samples in different higher grade categories, but the average D : O intensity ratios are distinguishable among the groups (Fig. 8a; see also Fig. 4 in Pasteris and Wopenka, 1991).

Our samples show a remarkable constancy in their S : O intensity ratios (Figs. 8b, 9), which typically range from 0.34 to 0.38, with slightly higher values (up to 0.47)

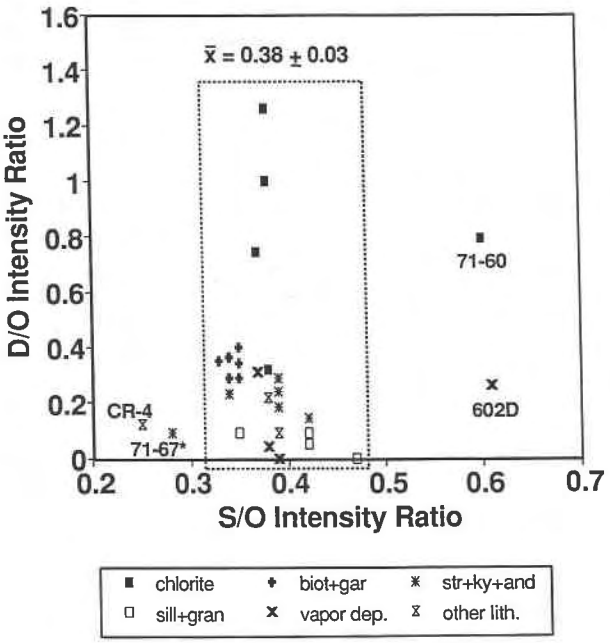

Fig. 9. Intensity ratio of D peak to O peak vs. intensity ratio of S peak to O peak. Graph includes all samples with second-order peaks, as listed in Table 2. Four unusual samples (see text) are labeled. Average S : O ratio and 1σ error are shown for all other samples (enclosed in dashed rectangle).

for sillimanite and granulite samples. We believe that the constancy of S : O reflects the covariation between degree of three-dimensional ordering (S peak) and the size of the coherent domains within the graphite basal planes (O peak). If this is true, then the lack of correlation of S : O with metamorphic grade supports a model of simultaneous increase in L_a and L_c. This interpretation is confirmed by HRTEM results in several samples from this study (Buseck and Huang, 1985; see below). In contrast, Ergun (1968) and Rouzaud et al. (1983) found no indication for simultaneous growth along the *a* and *c* axes in their samples. As seen in Figure 9, in terms of S : O ratio, four samples in our data set are unusual: two (CR-4 and 71-67*) have very low S : O intensity ratios, whereas two other samples (71-60 and 602D) have very high ratios. In the case of the CM coating on the inclusion wall of sample 602D, it was not possible to ensure that the incident beam of the laser was perpendicular to the surface of the graphite—in contrast to the geometry for samples CR-4, 71-67*, 71-60, and most of the other samples in this study. Thus, the observed differences in the intensity relationship between the first- and second-order spectrum of sample 602D may be a sampling artifact, e.g., caused by the fact that the second-order spectrum of graphite is strongly polarized with respect to the first-order spectrum (Nemanich and Solin, 1979). However, the development of the crystallite dimensions L_a and L_c in the other three unusual samples (Fig. 9) indeed seems to be atypical, i.e., different from all the other samples analyzed in this study. This conclusion is supported by the fact that all three of those samples were found to be unusual in other respects as well: 71-60 was the most heterogeneous sample in this study, 71-67* is one of two samples in this study for which there is an inconsistency in metamorphic grade assignment between the mineral assemblages and the Raman spectrum, and CR-4 is the only CM sample studied in a tuffaceous metaflysch host rock.

The major conclusion about quantification of the Raman spectral results on CM is that more than one or two parameters should be considered in order to interpret the degree of crystallinity of an isolated CM. For CM well enough crystallized to show second-order Raman peaks, the significant parameters that have to be evaluated are the position and width of the O peak and the D : O and S : O intensity ratios. For very poorly crystallized CM, however, such as kerogens, the evaluation of all of the latter spectral parameters is misleading rather than informative. Instead, the D peak width becomes the only quantifiable parameter representative of crystallite development. In addition, for any kind of CM, side by side viewing of entire CM spectra (both first- and, if present, second-order) is a very good means of simultaneously comparing numerous spectral parameters among different samples. In many cases, the eye can pick up on more subtleties of importance in CM maturity ranking than the evaluation of all possible calculable parameters does. Although this approach does not provide actual crystallite sizes, it does permit relatively accurate evaluation of the degrees of crystallinity of carbonaceous samples. The relative degree of CM crystallinity derived from Raman (or other) analysis can be interpreted in terms of metamorphic grades, at least for samples with identical host rocks. Additional information about the actual in-plane crystallite sizes in ångströms can be derived from the calibration curves published by Tuinstra and Koenig (1970a) and Beny-Bassez and Rouzaud (1985). We shall discuss in detail in a later section their methods of calibration and the application to our samples.

Comparison among different analytical techniques

The data available on our samples also permit comparisons among the results of different analytical techniques in terms of (1) the relative sensitivities of the techniques to the degree of crystallinity of CM, and (2) the different structural responses of CM to progressive graphitization. XRD of bulk carbonaceous separates is a classical means of determining graphite crystallinity. Figure 14 of Grew's (1974, p. 64) paper is a plot of XRD data on CM, including the samples subject to this study. It shows the relationship between peak width at half height for the (002) line and the apparent interplanar *d* values in ångströms, as derived from the (002) peak position. The peak width and *d* values show a large and almost linear decrease for samples throughout the chlorite (five samples), chloritoid (one sample), and biotite (one sample) zones. However, from the garnet through the silli-

manite zones, there is little change in the d values, whereas the peak width (in degrees 2θ) continues to change from about 0.46 to 0.18. (He also reported that the loss of H, O, and N in carbonaceous material is not complete below the staurolite zone.) According to Grew's (1974) XRD analyses, well-crystallized graphite ($d = 3.37$ Å) was attained by the high-grade portion of the chlorite zone. Thus, only the XRD peak widths correctly reflect the relative metamorphic grades of these samples. For instance, the d values for Grew's samples 71-56 (garnet zone) and 71-54 (sillimanite zone, not part of this study) are less than that for the highest grade metapelite (top of the sillimanite zone), 71-51, but it has the smallest peak width. On the other hand, XRD data for a sample of granulite-facies graphite from Sri Lanka depicted in the same diagram show an appreciably smaller d value than that of the rest of the samples but a greater peak width than the highest grade metapelite, 71-51. The metamorphic progression shown by the Raman spectra in Figure 2 of this paper is definitely less ambiguous than a plot of the XRD (002) peak widths against peak positions (Grew, 1974, his Fig. 14). As subsequently summarized by Rumble et al. (1977), conventional XRD data are very good indicators of metamorphic grade within the chlorite zone, but they become increasingly unreliable at higher grades. In contrast, there are noticeable changes in the Raman spectra even throughout the staurolite and sillimanite zones. Furthermore, granulite-facies material is distinguishable from amphibolite-facies (sillimanite-zone) graphite by the Raman spectra (see Table 2), but not by the XRD patterns (Grew, 1974, his Fig. 14). Samples from the opposite end of the range of crystallinity, i.e., kerogens and coals, provide another example of the limitations of the information that can be obtained from XRD. There exists a correlation between the H : C ratio (accurate reflection of the content of atoms other than C and, thus, maturity) and the degree of crystallinity of CM as derived from the XRD parameters of d values and peak width for the (002) reflection (e.g., Grew, 1974; Itaya, 1981; Hayes et al., 1983). Surprisingly, however, this correlation is frequently very poor (see e.g., Table 4 in Hayes et al., 1983). Again, it seems that the progression of the crystalline development shown by the Raman spectra in Figure 5 of this paper is less ambiguous than the information obtainable from conventional XRD analysis. The fact that Raman spectroscopy is superior to XRD analysis for the characterization of highly disordered CM can also be inferred from the presentation by Beny et al. (1986). The latter could not resolve an XRD (002) peak above background for an anthracite sample that had a very strong, quantifiable Raman spectrum.

Despite the above inconsistencies between the Raman and XRD results on very poorly and very well crystallized CM, the Raman and XRD data are in accord for samples of medium metamorphic grade. The latter correlation is demonstrated by two samples whose CM crystallinity suggests a higher metamorphic grade than the petrologic assignment. Sample 71-56 (Raman spectrum no. 23) gives an anomalously small d value and XRD peak width (Grew, 1974, see his Fig. 14 and Table 6) for a sample from the garnet zone, instead plotting with samples from the lower sillimanite zone. Grew (1974, p. 62) also commented that graphite from staurolite-zone sample 71-3 (Raman spectrum no. 25) of the Cockeysville marble (Maryland) has an XRD pattern similar to that for Sri Lanka graphite. As discussed above, the Raman spectra of these two samples place them in the staurolite and lower sillimanite zones, respectively (see Figs. 2 and 3). In another example, the graphite from mica schist 71-24 (Raman spectrum no. 20) indicates sillimanite-zone metamorphism by both analytical techniques, even though the sillimanite in the host rock has retrograded to sericite (Grew, 1974, p. 58).

In another study, Wintsch et al. (1981) did XRD and SEM analyses of graphite separates from metamorphosed arkoses collected in the same area of the Narragansett Basin from which Grew's (1974) samples come. However, the former analyzed graphite only from the chlorite, biotite, and garnet zones. They found little correlation between the grade of metamorphism of the host rock and the positions, widths, and shapes of the (002) XRD peak for graphite. Wintsch et al. (1981) concluded from their data that the XRD peaks instead are strong functions of the grain size and grain size distribution of the graphite. In contrast with XRD, LRM analysis does not appear to be sensitive to grain size (as distinguished from crystallite size).

Comparisons also can be made between the HRTEM analyses (Buseck and Huang, 1985) and LRM analyses (this work) done on 16 metapelites, eight of which were studied in detail by HRTEM (Sh-2, 71-46, Sh-1, 68-1, 71-8, 71-65, 71-53, and 71-56). The results of this sequence clearly point out that the extremely high resolution of the TEM technique actually has a disadvantage: in order to evaluate the overall degree of crystallinity of a sample, numerous mounts and observations must be made. The eventual interpretation of HRTEM observations is quite subjective, and Buseck and Huang (1985) do not report any actual crystallite dimensions. Therefore, their HRTEM observations do not lend themselves to a straightforward sample by sample comparison with the Raman data, and unfortunately cannot be used to check existing calibrations of Raman spectra in terms of L_a (Tuinstra and Koenig, 1970a; Beny-Bassez and Rouzaud, 1985; see later discussion). However, in general, the metamorphic grade sequences inferred by the HRTEM and the Raman technique agree very well, despite the differences in both the analytical information and the scale for these two techniques (Table 1). The only sample found to be very heterogeneous in our Raman study (71-60) also displayed a wide range of crystallinity in the HRTEM observations (Buseck and Huang, 1985). The fact that the degree of crystallinity inferred by means of both techniques is the same for all of the samples studied is another indication that L_a and L_c indeed developed simultaneously in those samples, as we already had concluded from

their rather uniform S : O Raman peak intensity ratios (see above).

Buseck et al. (1988) analyzed four other samples by HRTEM that subsequently were subjected to this Raman study, i.e., kerogen samples 123-1-RK, 114-1-RK, 498-1-RK, and 027-1-RK. The most obvious observation from Figure 5 is that the LRM spectra of the chert-hosted and the shale-hosted kerogens are fundamentally different. The sequence of increasing structural order, as determined by HRTEM analysis of shale-hosted kerogens (114-1-RK, 123-1-RK, 498-1-RK), is the same as that inferred by LRM analysis from the decreasing D peak widths (see Table 2). Although the D : O intensity and D : O area ratios of chert-hosted sample 027-1-RK are very similar to the one of shale-hosted 123-1-RK, the former's D peak width is considerably narrower than those of the shale-hosted CM. As stated above, for kerogens and coals, it is the D peak width that best indicates their structural order.

The comparison of compositional, XRD, HRTEM, and LRM data on these several kerogens indicates poor correlation between XRD parameters and composition (table of pertinent data available from authors; data extracted from Tables 5-7 and 5-8 in Hayes et al., 1983), as well as between XRD parameters (Hayes et al., 1983), and both HRTEM (Buseck et al., 1988) and LRM data (this work). The HRTEM data correlate quite well, however, with the observed degree of metamorphism of the host rock. For kerogens with the same host rock, the Raman D peak width correlates excellently with the recorded degree of metamorphism, H : C ratio, and HRTEM observations on degree of structural order. In addition, it appears from our small sample that the Raman spectra of shale-hosted and chert-hosted kerogens may be fundamentally different.

In another study, Wang et al. (1989) characterized seven carbonaceous samples (with a range from very little to no disorder) associated with a U deposit by Raman microsampling spectroscopy, XRD, HRTEM, and SEM. Their comparison of the different analytical techniques is in accord with ours: they did not find the XRD method well suited, since they barely found a difference in the XRD spectra among their samples. In contrast, both second-order Raman spectra and HRTEM measurements were informative and showed a small loss of structural ordering along the c axis in the same samples. The approach of Wang et al. (1989), of using multiple analytical techniques, also pointed out the advantages and high sensitivity of the Raman technique for pinpoint in situ measurements of surficial disorganization and localized defects in CM.

In summary, Raman microsampling spectroscopy appears to be more sensitive than XRD measurements of (002) peak position and peak width in the ranking of CM by its maturity. Furthermore, the Raman microprobe, with its spatial resolution on the order of micrometers, has the potential to identify heterogeneities in crystallinity that would not be identifiable by XRD analysis of bulk graphite. When comparing the results of different techniques, it must be kept in mind, however, that the perception of ordering in graphite in part reflects the kind of structural information that is available. In conventional Raman terminology, "disorder" means a small crystallite size in terms of L_a, without suggesting whether stacking disorder also exists. In contrast, HRTEM lattice-fringe images allow one to distinguish between the extent and degree of crystal perfection along the **c** axis (what electron microscopists typically call "ordering"), whereas reported XRD data typically only include position (and, in some cases, width) of the (002) reflection, which is interpreted as the distance between two aromatic planes, i.e., d values (what X-ray analysts typically call "ordering").

Calibration of Raman spectra by means of XRD and HRTEM results

Most Raman papers that provide L_a values for CM rely on the original correlation chart of Tuinstra and Koenig (1970a). The latter studied the intensity ratio of the Raman first-order D and O peaks ($I_{\approx 1355\ cm^{-1}}/I_{\approx 1600\ cm^{-1}}$) as a function of in-plane crystallite size L_a (determined by means of XRD analysis) and found a linear relationship between $1000/L_a$ (Å) and the Raman intensity ratio. Their calibration curve is based on seven CM samples with L_a values between 38 and 300 Å (D : O intensity ratios between 1.02 and 0.105), and one additional sample with L_a = 2250 Å, which has a D : O intensity ratio of only 0.02. (The authors did not list those numbers explicitly; they are derived from their Fig. 3.) Tuinstra and Koenig (1970a, 1970b) did not document how they evaluated the independent XRD analyses to derive the L_a values ultimately used to calibrate their Raman spectral results. This is unfortunate, because even for well-crystallized graphite, the determination of L_a from the XRD (110) lattice reflection is not an easy task, e.g., several corrections for instrumental and strain broadening effects are necessary (Ergun, 1968). The determination becomes even less straightforward for microcrystalline (disordered) forms of CM, which give rise to diffuse bands. According to Ergun (1968), the results for L_a and L_c that are determined from X-ray reflections may be regarded as only order-of-magnitude values. Indeed, Tuinstra and Koenig's work (1970a, 1970b) could not be reproduced by other authors (e.g., Nakamizo et al., 1974; Tsu et al., 1978), mainly because of the difficulty in obtaining reliable values of L_a from XRD data. According to Nakamizo et al. (1974), the kind of material that has an observable D peak in its Raman spectrum has such "extremely weak and broad x-ray diffraction peaks from the (110) plane, so as to render the determination of L_a values unfeasible [sic]" (p. 262). The latter may account for discrepancies among experimental XRD studies. In agreement with Tuinstra and Koenig, Nakamizo et al. (1974) still saw a disorder-induced peak in CM (crudely pulverized graphite) with an L_a value of 1500 Å (as measured by XRD line broadening). However, for the same observed intensity ratio of Raman bands, Tsu et al. (1978) reported L_a values [also based

on analysis of X-ray line widths of the (110) reflection] that are generally an order of magnitude larger than those reported by Tuinstra and Koenig (1970a). To make matters even more confusing, all three of those experimental Raman and X-ray studies are in contradiction to the calculations made by Lespade et al. (1982), who predicted that only material with an in-plane crystallite size, L_a, of $< \approx 100$ Å would have disorder-induced peaks in the Raman spectrum.

It also appears that Tuinstra and Koenig's (1970a) plot of peak intensity ratios combined data from samples oriented in several ways with respect to the incident laser beam. Although they apparently recorded most of their Raman spectra on crystals oriented with their basal planes perpendicular to the laser beam, their microcrystalline samples were pressed into pellets and irradiated with a beam that was 60° from perpendicularity. Indeed, Tuinstra and Koenig (1970a, p. 1126) reported that "different orientation of the sample with respect to the incident beam did not change the spectrum. Polarization measurements were attempted but no polarization was detected [in the first-order spectrum]." Wang et al. (1989) have shown, however, that when the beam direction is changed from 90 to 45° with respect to the basal plane of a coarse graphite flake, the Raman spectrum shows an increase of 0.15 in the D : O intensity ratio. This increase translates into a perceived L_a difference of several hundred ångströms, as interpreted from Tuinstra and Koenig's (1970a) plot. Pasteris (1989) has pointed out that these recorded differences in D : O ratios as a function of grain orientation cause large apparent variations in L_a for well-crystallized material, but only small variations for disordered CM (because of the functional relationship between L_a and D : O), probably mitigating the effects on Tuinstra and Koenig's (1970a) data. However, as pointed out by Chieu et al. (1982), D : O intensity ratios below about 0.2 (corresponding to an L_a of about 200 Å according to Tuinstra and Koenig, 1970a), are extremely difficult to quantify. Further confusion has ensued as some subsequent authors (e.g., Fitzer et al., 1987) have interpreted their D : O peak area ratios using Tuinstra and Koenig's (1970a) plot of peak intensity ratios of D : O.

The above discussion explains why a quantitative Raman spectral determination of L_a has led to considerable confusion and interlaboratory discrepancy. The HRTEM work of Beny-Bassez and Rouzaud (1985) fortunately satisfied the need for a different means of calibrating the Raman spectra of CM, given the obvious difficulty in obtaining accurate L_a values by means of XRD analysis. Beny-Bassez and Rouzaud's (1985) study proved that it is the XRD data of Tuinstra and Koenig (1970a) that are reliable. In their combined HRTEM-Raman study, the former used three different types of artificial CM (anthracene cokes, thin C films, and thick C films), which they heat treated up to 3000 °C in 100 °C steps in order to produce a total of 49 CM samples with a wide range of crystalline development. Beny-Bassez and Rouzaud (1985) used HRTEM to measure L_a values directly from lattice-

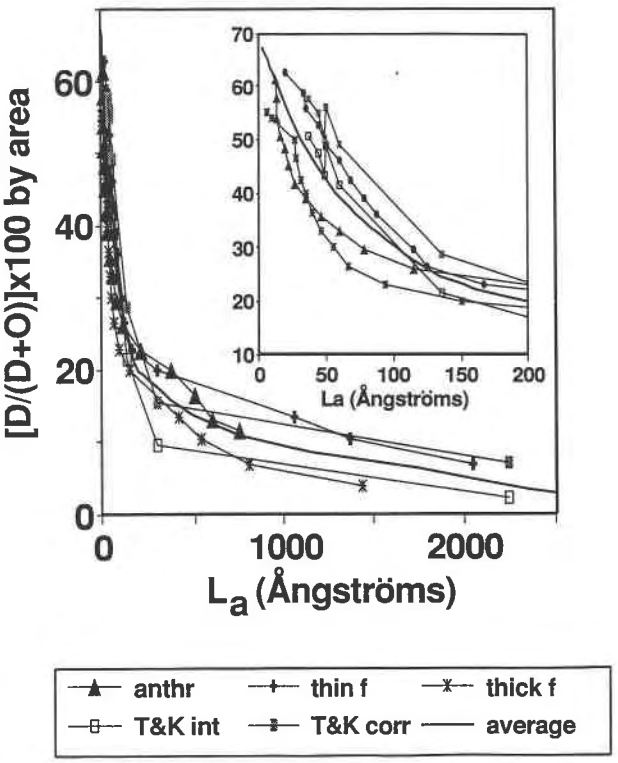

Fig. 10. Specific area of D-band (see text) approximated by area of D peak over sum of areas of D and O peaks, multiplied by 100, vs. in-plane crystallite size L_a in ångströms. Points for anthracene cokes (anthr), thin C films (thin f), and thick C films (thick f) are derived from Beny-Bassez and Rouzaud's (1985) calibration data by means of HRTEM (110) dark-field micrographs. For comparison, Tuinstra and Koenig's (1970a) calibration data by means of XRD (originally plotted as D : O intensity ratios) are represented as peak intensity ratios (T&K int), and as peak area ratios (T&K corr). Conversion from intensity to area ratios is based on a correlation found in samples from this work [D : O intensity ratio = 0.78 × (D : O area ratio)]. Also shown is our visually derived average calibration curve (solid line without symbols), used to estimate in-plane crystallite sizes for samples in this study.

fringes and (110) dark-field micrographs. They correlated those in-plane crystallite sizes [plotted as $1000/L_a$ (Å)] with the Raman spectroscopic parameter S_{1350}, which they defined on page 119 as "the specific surface of the Raman band characteristic of the defects centered at about 1350 cm^{-1}, i.e., ratio between surfaces of this band and the whole spectrum." They published three diagrams, i.e., for anthracene cokes, thin C films, and thick C films. We have denoted Beny-Bassez and Rouzaud's (1985) S_{1350} parameter as the peak area ratio [D/(D + O)] × 100, which it approximates, and have replotted their calibration data in a different format in our Figure 10. For comparison, we also converted Tuinstra and Koenig's (1970a) calibration data (originally plotted as D : O intensity ratios) into values of [D/(D + O)] × 100 based on peak intensities (open squares in Fig. 10) and on peak areas (filled squares in Fig. 10). The latter area ratios were in-

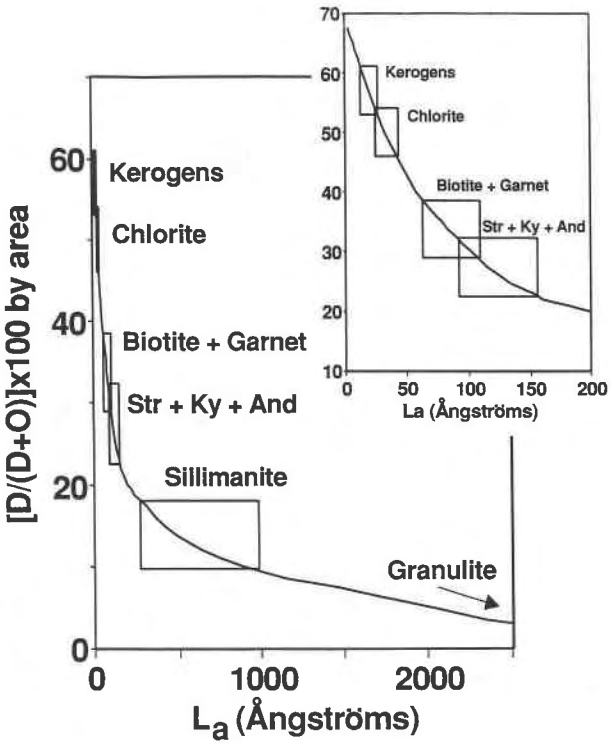

Fig. 11. Correlation curve between specific area of D peak (approximated by [D/(D + O)] × 100, where D is the peak area of the peak at ≈1355 cm^{-1}, and O is the peak area of the peak at ≈1600 cm^{-1}) and in-plane crystallite size L_a. Correlation curve, i.e., average calibration curve, is derived from original data by Tuinstra and Koenig (1970a) and Beny-Bassez and Rouzaud (1985), as shown in Fig. 10. Rectangles represent the average value for 1σ error for the specific area of the D peak for each metamorphic category listed; corresponding L_a values defined from our average calibration curve (solid curve without symbols, as shown in Fig. 10). Inset (enlargement) shows specific ranges in in-plane crystallite size, L_a, for CM from the four lowest grade metamorphic categories in this study.

ferred from Tuinstra and Koenig's (1970a) intensity ratios by means of the observed correlation between these parameters in our own samples. As seen in Figure 10, Beny-Bassez and Rouzaud's (1985) calibration curves derived from direct HRTEM measurements of L_a values agree well with our representation of Tuinstra and Koenig's (1970a) original data, which were based on indirect determinations of L_a by means of empirical XRD methods. Several factors led us to visually derive an average calibration curve from all the available calibration data (solid line without symbols in Figs. 10 and 11): there is a surprisingly good agreement between the XRD- and HRTEM-based calibration curves. The precursors for most natural samples are unknown or of mixed origin, thus precluding the accurate choice of one of Beny-Bassez and Rouzaud's curves, and we wanted to estimate the in-plane crystallite sizes L_a for the samples studied in this work (see Table 2 and Fig. 11). It is difficult, if not impossible, to determine the uncertainties associated with the L_a values derived from our average calibration curve. Firstly, the uncertainties in the original calibration data are unknown. Secondly, although each of the original calibration curves shown in Figure 10 is consistent with the average curve, reference to the highest and lowest individual curves for any given S_{1350} parameter yields L_a values that differ by about 70% (relative) from each other. Thirdly, the difficulty and inaccuracy in measuring areas of both broad peaks and very small peaks will increase the uncertainties in S_{1350} parameters for very poorly ordered and very well-ordered CM, respectively.

Implications for the process of graphitization of natural carbonaceous material

There are still major questions concerning the process and progress of graphitization, such as its generalizability, precursor dependence, continuity, and bulk compositional control. Raman spectroscopy previously has been applied to coals (e.g., Beny-Bassez and Rouzaud, 1985; Beny et al., 1986) and kerogens (Beny and Jehlicka, 1989; Landais et al., 1990). There also are miscellaneous Raman analyses of other natural carbonaceous materials (e.g., Christophe Michel-Levy and Lautie, 1981; Guilhaumou et al., 1984; Pasteris et al., 1986; Pasteris, 1988; Wopenka, 1988; Wang et al., 1989), but more broadly based tests of the geologic applicability of Raman spectroscopy of CM have been made only recently (Pasteris and Wopenka, 1991) and are the subject of this paper. The comparison of the above with results obtained on artificially produced CM allows us to address the question of generalizability, i.e., whether natural carbonaceous materials graphitize by the same process as simpler organic compounds undergoing heat treatment. Under "process" we include mechanism, sequence of stages of development, and functional relationship among the crystallographic parameters during development.

The comparison of Raman spectra of CM from this paper with those of artificially produced highly oriented pyrolitic graphite, glassy C, pressed C rods, and C powders, which are reported by Nemanich and Solin (1979, their Fig. 8, p. 398), shows a strong resemblance in both the first- and second-order spectral features and in the codevelopment of those features. However, spectra of other heat-treated CM of various origins (e.g., Vidano and Fischbach, 1978; Nemanich and Solin, 1979; Chieu et al., 1982; Rouzaud et al., 1983; Beny-Bassez and Rouzaud, 1985; Beny et al., 1986; Knight and White, 1989), such as organic compounds, methane gas, and coals, can differ from the spectra of our natural CM in various spectral details. For instance, in comparisons among samples with similar D : O ratios, natural CM samples show both better resolution in their second-order S peak and significantly narrower O peak widths than do benzene-derived C fibers that were heat-treated between 1100 and 2900 °C (Chieu et al., 1982). This result implies that three-dimensional ordering may be facilitated in natural samples, which are not only subjected to high temperatures

but also to other catalytic effects such as high pressure. Particularly in their lack of a discernible second-order Raman spectrum, the spectra of the benzene-derived C fibers studied by Chieu et al. (1982) resemble those of our kerogens and coals, as well as the synthetically produced sample AA3. Overall, the process of graphitization seems to be a general one in that the mechanism and the sequence of stages leading from structural disorder to order is the same (or at least very similar) in both natural and artificial materials. It therefore is not possible to discriminate among naturally and artificially produced carbonaceous materials solely by comparison of their respective Raman spectra.

Our limited data suggest, however, that fluid-deposited CM develop differently in response to deposition temperature than do organic precursors undergoing heat treatment. This suggestion is in accord with some observations made by Reutel (1992), who presented TEM images and the first-order Raman spectra for several CM samples representing both metamorphosed organic matter (for which C isotope thermometry provides temperature estimates) and fluid-deposited C. He reported problems in interpreting the temperature of equilibration of the fluid-deposited CM by reference to the Raman spectra from the metamorphic samples.

For CM well enough crystallized to have a second-order Raman spectrum, the development from structural disorder to order seems to follow the same nonspecific process, i.e., independent of any specific precursor chemistry. However, this does not seem to be the case for very poorly crystallized CM. Instead, many pathways (specific sequences of development) seem to be possible at the very early stage of crystallite development, i.e., before the onset of three-dimensional structural order. Such different pathways are reflected, e.g., by curves of different slopes in diagrams plotting any crystallite-size parameter (such as L_a, L_c, d, derived, e.g., by XRD) vs. any intensive thermodynamic variable related to metamorphism (e.g., temperature). The different pathways all seem to meet, however, once the in-plane crystallite size L_a reaches about 30 Å (i.e., the approximate minimum L_a value for our CM that demonstrates second-order peaks; see Table 2) and three-dimensional ordering starts (i.e., reflected by appearance of second-order peaks). From then on, graphitization seems to occur by the same process, independent of the specific precursor chemistry. For instance, the spectra in Figures 2–4 and our interpretation of the relationship between measured spectral parameters and metamorphic grade (see Table 2) demonstrate that the covariation of L_a and L_c (i.e., the lack of variation in the S : O intensity ratio with metamorphic grade) is very similar over the recorded metamorphic range.

Both among researchers investigating natural CM and those studying heat-treated synthetic suites of CM, there has been disagreement about whether graphitization is a continuous process or one that occurs in several discrete steps. Among geologists doing extensive XRD analysis, Grew (1974) and Itaya (1981) reported evidence for a continuous process, but Landis (1971) described discrete steps. Based on their HRTEM studies on natural material (Buseck and Huang, 1985) and on artificial carbonaceous materials (Beny-Bassez and Rouzaud, 1985), the former researchers inferred a continuous process of graphitization, whereas the latter (who also did Raman analyses and established the calibration curves shown in Fig. 10) recognized three discrete steps in graphite development. Any discontinuities in the graphitization process are important factors in the structural and compositional equilibration of CM, which can have an impact on the interpretation of the structural order of CM, as well as of the C isotope fractionation between mineral pairs or between graphite and fluid.

An important factor in the perception of discontinuity is how the rate of change of the crystallite parameters (L_a, L_c, d) varies in response to precursor chemistry, temperature, and pressure. It is known that distinctive types of organic precursor CM mature differently, i.e., at different rates, particularly at the lowest grades of metamorphism (Tissot and Welte, 1984). Thus, it is plausible to assume that graphitization at the very early stages of two-dimensional ordering proceeds not only along different pathways (as discussed above), but also at different rates. Our Raman data further suggest that the relationship between temperature and L_a (and L_c, since they seem to covary) is not constant for more mature CM. Figure 11 indicates that in carbonaceous pelites undergoing progressive metamorphism, the increase in crystallite size (L_a) is relatively small throughout low and intermediate grades of metamorphism. Upon attainment of upper amphibolite grade (sillimanite zone), however, the in-plane crystallite size increases very readily and attains values about an order of magnitude greater than those in the staurolite + kyanite + andalusite zones. In addition, the S : O intensity ratios, which are a reflection of three-dimensional ordering, tend to be slightly higher for sillimanite and granulite samples (Fig. 9). A reasonable corollary to these observations is that some kinetic barrier is overcome at conditions approximated by those in the sillimanite zone. The latter hypothesis would also explain why there are so few calibration products with L_a values between about 800 and 2000 Å (see Fig. 10), i.e., because it is difficult to halt crystallite enlargement at this step in the progression. (Unfortunately, we do not have a sufficient number of samples that crystallized at the same temperature but at different pressures to evaluate whether or not the higher pressures in the kyanite-sillimanite facies series facilitates graphite crystallization relative to the andalusite-sillimanite facies series.)

Another question, touched on by Grew (1974), is whether graphitization proceeds more readily in some host rocks (namely carbonates) than in others (such as coal, black slate, pelites). The Raman data on two adjacent shungite samples (Sh-1 and Sh-2, Fig. 2A) indicate how the rock matrix (CM dispersed in chert and more massive coal, respectively) has affected the progress of graphitization: the CM in chert is much better ordered. Our Ra-

man data also confirm that at the same grade of metamorphism there is a higher degree of crystallinity in CM samples in calcareous rocks (71-56 and 71-3, Fig. 3) and in the metaflysch sample CR-4 than in samples hosted in metapelites. Our data also indicate better structural development in kerogens hosted in chert than in shale (Fig. 5), although the metamorphic grades also may differ among these samples.

There are two possible explanations for the bulk compositional control on the efficiency of graphitization: (1) Graphitization is affected by the composition of the volatiles produced by the (probably buffered) reaction of the organic matter and its rock matrix during heating. Wintsch et al. (1981) inferred that the f_{CH_4} and f_{H_2} values were important controls on the degree of graphite crystallinity in the metamorphosed arkoses that they examined. Their hypothesis is based on the fact that a major process in graphitization is the expulsion of heteroatoms of O, H, and N. For their rocks, as well as the current suite, the effectiveness of this expulsion process is a function of the fugacities of O-, H-, and N-bearing gases (see, e.g., Fig. II.5.1 of Tissot and Welte, 1984, p. 161), as well as the permeability of the host rock. (2) Different types of precursor organic matter would be expected to accumulate in sedimentary sequences characterized by different rock types, e.g., pelite vs. carbonate vs. chert. The fact that the rate of graphitization is a function of the host rock, however, while limiting the usefulness of CM as a metamorphic indicator, does not decrease the usefulness of the Raman spectroscopic or any other technique to characterize such materials.

Summary and conclusions

Raman microsampling spectroscopy of CM provides information similar to that obtained from XRD and HRTEM analysis, but on an intermediate sample-size scale (Table 1). Furthermore, Raman microsampling spectroscopy can be done relatively rapidly, for the most part nondestructively, in situ (in a rock or thin section), or on grain separates. In the latter regard, the laser Raman microprobe technique overcomes a major disadvantage of HRTEM and XRD analyses, which require the removal of the CM from its textural context. Some samples from this study, particularly graphitic coatings on the walls of fluid inclusions, probably could not have been analyzed by XRD or HRTEM (e.g., AA3 and 602D).

However, the Raman data suffer from the same limitation as the XRD and HRTEM data on graphite: none of the techniques can provide a generalized correlation between analytical output (e.g., XRD pattern or lattice-fringe image) and degree of metamorphism of the host rock. That is because differences in carbonaceous precursors and differences in host rocks have a recognized effect on the degree of crystallinity attained by CM under any given P-T conditions. Thus, in terms of inferring metamorphic grade, the geological usefulness and applicability of doing Raman microsampling spectroscopy on CM ultimately are constrained by how well the actual physical properties of graphite reflect the conditions under which it crystallized or recrystallized. Some of the complexity of the latter considerations is eliminated in the part of this study addressing Grew's (1974) samples, because the majority of them are metapelites. For this suite of rocks, it is of interest that the sequencing of the Raman spectra according to crystallinity correlates excellently with Grew's (1974) mineralogically inferred metamorphic grade. The graphitization process of the CM in this suite of rocks seems to be independent of the specific organic precursors, given that the latter includes both marine and nonmarine materials. Our Raman work suggests that once recognizable three-dimensional ordering is attained (i.e., second-order Raman spectral features occur), the process of graphitization is very similar for all materials.

Several important generalizations can be drawn from the Raman spectra of carbonaceous materials analyzed in this study. The Raman spectrum is sensitive to the degree of crystallinity of CM ranging from kerogen and coal to granulite-grade graphite (see Fig. 11). In contrast to XRD-derived data, they even can be used to distinguish among samples of high and very low metamorphic grades. The grouping and sequencing of individual metapelites and kerogens by Raman analysis are essentially the same as those inferred from independent HRTEM analyses (Buseck and Huang, 1985; Buseck et al., 1988). All three techniques (HRTEM, XRD, Raman) indicate major changes in overall graphite structure within the chlorite-zone samples.

Our results strongly suggest that, given the actual first- and second-order Raman spectra of graphitic standards from samples of known metamorphic grade, one could pinpoint the metamorphic grade of another similar sample of the same rock type based solely on the Raman spectrum of its carbonaceous matter. In addition, the Raman calibrations established by Tuinstra and Koenig (1970a) and Beny-Bassez and Rouzaud (1985) enable the estimation of in-plane crystallite sizes L_a for any given sample of CM, regardless of rock type (Fig. 10). To our knowledge, Figure 11 is the first representation of the range and absolute values of L_a of a natural suite of graphitic rocks. The correlation shown in this figure between the average calibration curve (for Raman data) and the metamorphic zones of CM samples permit the degree of metamorphism of a metapelite host rock to be inferred from the Raman-derived value of L_a.

Most significantly, the possibility with the LRM to do grain by grain (especially, in situ) determination of the state of structural order of carbonaceous material can lead to important conclusions and provide various geologic constraints. (1) The recognition of (the degree of) disorder in CM precipitates in fluid inclusions, hydrothermal CM in a rock matrix, and metamorphosed CM is essential to the accurate determination of f_{O_2} of a system and, thus, the speciation of the ambient fluid. As discussed theoretically by Ziegenbein (1979) and applied geologically by Ziegenbein and Johannes (1990), for the C-O-H system at any given P and T, the field of graphite saturation is

smaller for poorly ordered than for well-ordered graphite. There are at least two important ramifications of this relationship. At fixed P and T, the coexistence of graphite and a C-O-H fluid occurs at more reducing conditions in the presence of poorly ordered than well-ordered graphite. There are various reports in the literature of the inferred failure of graphite to precipitate under T-P-f_{O_2} conditions calculated to induce saturation with respect to well-ordered graphite. Although in some cases this situation is due to kinetic inhibition of graphite precipitation, in other cases it may reflect a lack of saturation with respect to poorly ordered graphite, which is the more likely initial precipitation product. (2) Because of the structural and f_{O_2} differences between the coexistence of carbonate with poorly ordered compared with well-ordered graphite, it is likely that there will be differences in C isotope fractionation between those two situations. The recognition of different degrees of order in graphite, coupled with theoretical modeling or experimental data on isotope fractionation, would permit increased accuracy in C isotope thermometry. (3) Our small sample of fluid-deposited graphite permits some comparisons between CM samples that have been graphitized and those that were deposited from a fluid under the same P-T conditions. Such comparisons aid the interpretation of the origin of different types of graphite, such as those revealed by spectroscopic mapping of variations in the degree of crystallinity among graphite grains within a given thin section (e.g., Wopenka et al., 1988). For instance, if the metamorphic assemblage of a sample clearly points to a single equilibration event, it may be reasonable to infer the coexistence of both thermally matured organic matter and fluid-deposited graphite to explain consistent contrasts in crystallinity.

Acknowledgments

The authors are grateful to Robert Bodnar, I-Ming Chou, Maria Luisa Crawford, John Hayes, Michael Sterner, Harald Strauss, E-an Zen, and especially Edward Grew for the loan of samples. Edward Grew also supplied additional unpublished information on his samples. They thank John Foote and Jeffery Seitz for assistance with sample handling, Thomas Bernatowicz for HRTEM analyses, and Steven Dunn and Claire Beny for reviews of an earlier version of the manuscript. The authors accept full responsibility for all data and interpretations presented. This work was supported in part by NSF grants EAR-8817050 and EAR-9023520 and by a NASA innovative grant, NAGW122.

References cited

Allamandola, L.J., Sandford, S.A., and Wopenka, B. (1987) Interstellar polycyclic aromatic hydrocarbons and carbon in interplanetary dust particles and meteorites. Science, 237, 56–59.

Arneth, J.D., Schidlowski, M., Sarbas, B., Goerg, U., and Amstutz, G.C. (1985) Graphite content and isotopic fractionation between calcite-graphite pairs in metasediments from Mgama Hills, Southern Kenya. Geochimica et Cosmochimica Acta, 49, 1553–1560.

Baker, A.J. (1988) Stable isotope evidence for limited fluid infiltration of deep crustal rocks from the Ivrea Zone, Italy. Geology, 16, 492–495.

Ballhaus, C.G., and Stumpfl, E.F. (1985) Occurrence and petrological significance of graphite in the Upper Critical Zone, western Bushveld Complex, South Africa. Earth and Planetary Science Letters, 74, 58–68.

Beny, C., and Jehlicka, J. (1989) Applications de la microspectrométrie Raman à l'étude de la graphitation naturelle de kerogènes Précambriens. Abstracts of the symposium GEORAMAN, May, 1989, Toulouse, France, 89, 1–2.

Beny, C., Oh, J.H., and Rouzaud, J.N. (1986) La formation du graphite: Un domaine d'application pour la microspectrometrie RAMAN. Principaux resultats scientifiques et techniques du BRGM, 1986, 247–248.

Beny-Bassez, C., and Rouzaud, J.N. (1985) Characterization of carbonaceous materials by correlated electron and optical microscopy and Raman microspectroscopy. Scanning Electron Microscopy, 1985, 119–132.

Bonijoly, M., Oberlin, M., and Oberlin, A. (1982) A possible mechanism for natural graphite formation. International Journal of Coal Geology, 1, 283–312.

Bottinga, Y. (1969) Calculated fractionation factors for carbon and hydrogen isotope exchange in the system calcite–carbon dioxide–graphite–methane–hydrogen–water vapor. Geochimica et Cosmochimica Acta, 33, 49–64.

Buseck, P.R., and Huang, B.-J. (1985) Conversion of carbonaceous material to graphite during metamorphism. Geochimica et Cosmochimica Acta, 49, 2003–2016.

Buseck, P.R., Huang, B.-J., and Keller, L.P. (1987) Electron microscope investigation of the structures of annealed carbons. Journal of Energy and Fuels, 1, 105–110.

Buseck, P.R., Huang, B.-J., and Miner, B. (1988) Structural order and disorder in Precambrian kerogens. Organic Geochemistry, 12, 221–234.

Chacko, T., Mayeda, T.K., Clayton, R.N., and Goldsmith, J.R. (1991) Oxygen and carbon isotope fractionations between CO_2 and calcite. Geochimica et Cosmochimica Acta, 55, 2867–2882.

Chieu, T.C., Dresselhaus, M.S., and Endo, M. (1982) Raman studies of benzene-derived graphite fibers. Physical Review B, 26, 5867–5877.

Chou, I-Ming (1987) Calibration of the graphite-methane buffer using the f_{H_2} sensors at 2 kilobar pressure. American Mineralogist, 72, 76–81.

Christophe Michel-Levy, M., and Lautie, A. (1981) Microanalysis by Raman spectroscopy of carbon in the Tieschitz chondrite. Nature, 292, 321–322.

Deurbergue, A., Oberlin, A., Oh, J.H., and Rouzaud, J.N. (1987) Graphitization of Korean anthracites as studied by transmission electron microscopy and x-ray diffraction. International Journal of Coal Geology, 8, 375–393.

Diessel, C.F.K., and Offler, R. (1975) Change in physical properties of coalified and graphitised phytoclasts with grade of metamorphism. Neues Jahrbuch für Mineralogie Monatshefte, 1975, 11–26.

Diessel, C.F.K., Brothers, N.R., and Black, P.M. (1978) Coalification and graphitization in high-pressure schists in New Caledonia. Contributions to Mineralogy and Petrology, 68, 63–78.

Dresselhaus, M.S., and Dresselhaus, G. (1982) Light scattering in graphite intercalation compounds. In M. Cardona and G. Guntherodth, Eds., Light scattering in solids, p. 3–57. Springer-Verlag, New York.

Duke, E.F., and Rumble III, D. (1986) Textural and isotopic variations in graphite from plutonic rocks, south-central New Hampshire. Contributions to Mineralogy and Petrology, 93, 409–419.

Dunn, S.R., and Valley, J.W. (1988) Calcite-graphite carbon isotope exchange during metamorphism; south-central Maine and southern Ontario. Geological Society of America Abstracts with Programs, 20, 46.

——— (1992) Calcite-graphite isotope thermometry: A test for polymetamorphism in marble, Tudor gabbro aureole, Ontario, Canada. Journal of Metamorphic Geology, 10, 487–501.

Elman, B.S., Dresselhaus, M.S., Dresselhaus, G., Maby, E.W., and Mazurek, H. (1981) Raman scattering from ion-implanted graphite. Physical Review B, 24, 1027–1034.

Elman, B.S., Shayegan, M., Dresselhaus, M.S., Mazurek, H., and Dresselhaus, G. (1982) Structural characterization of ion-implanted graphite. Physical Review B, 25, 4142–4156.

Ergun, S. (1968) X-ray studies of coals and carbonaceous materials. U.S. Bureau of Mines Bulletin, 648, 35 p.

Fitzer, E., Gantner, E., Rozploch, F., and Steinert, D. (1987) Application of laser-Raman spectroscopy for characterization of carbon films. High Temperatures–High Pressures, 19, 537–544.

French, B.M. (1964) Graphitization of organic material in a progressively metamorphosed Precambrian iron formation. Science, 146, 917–918.

———(1966) Some geological implications of equilibriums between graphite and a C-H-O gas phase at high temperatures and pressures. Reviews in Geophysics, 4, 223–253.

Grew, E.S. (1974) Carbonaceous material in some metamorphic rocks of New England and other areas. Journal of Geology, 82, 50–73.

Grew, E.S., and Day, H.W. (1972) Staurolite, kyanite, and sillimanite from the Narragansett basin of Rhode Island. U.S. Geological Survey Professional Paper 800-D, D151–D157.

Guilhaumou, F., Velde, B., and Beny, C. (1984) Raman microprobe analysis of gaseous inclusions in diagenetically recrystallized calcites. Bulletin de Minéralogie, 107, 193–202.

Haaland, D.M., Higgins, K.L., and Tallant, D.R. (1990) Multivariate calibration of carbon Raman spectra for quantitative determination of peak temperature history. Vibrational Spectroscopy, 1, 35–40.

Hayes, J.M., Kaplan, I.R., and Wedeking, K.W. (1983) Precambrian organic geochemistry, preservation of the record. In J.W. Schopf, Ed., Earth's earliest biosphere: Its origin and evolution, p. 93–134. Princeton University, Princeton, New Jersey.

Hess, N., Ghose, S., and Ganguly, J. (1988) Detection of submicroscopic graphites in charnockites from southern India by Raman spectroscopy and its petrological significance (abs.). Eos, 69, 1514.

Hoefs, J., Strakenbrock, I., and Ahrendt, H. (1988) Isotope investigations (C, O) of lower crustal rocks from the Ivrea Zone, Italy: The calcite-graphite thermometer and evidence for heterogeneous fluid interactions. V.M. Goldschmidt Conference: Program and Abstracts, 48.

Hollister, V.F. (1980) Origin of graphite in the Duluth Complex. Economic Geology, 75, 764–766.

Holloway, J.R. (1984) Graphite-CH_4-H_2O-CO_2 equilibria at low-grade metamorphic conditions. Geology, 12, 455–458.

Itaya, T. (1981) Carbonaceous material in pelitic schists of the Sanbagawa metamorphic belt in central Shikoku, Japan. Lithos, 14, 215–224.

Jedwab, J., and Boulegue, J. (1984) Graphite crystals in hydrothermal vents. Nature, 310, 41–43.

Katagiri, G., Ishida, H., and Ishitani, A. (1988) Raman spectra of graphite edge planes. Carbon, 26, 565–571.

Katz, M.B. (1987) Graphite deposits of Sri Lanka: A consequence of granulite facies metamorphism. Mineralium Deposita, 22, 18–25.

Kelly, B.T. (1981) Physics of graphite, p. 1–470. Applied Science Publishers, New York.

Knight, D.S., and White, W.B. (1989) Characterization of diamond films by Raman spectroscopy. Journal of Material Research, 4, 385–393.

Landais, P., Dubessy, J., Poty, B., and Robb, L.J. (1990) Three examples illustrating the analysis of organic matter associated with uranium ores. Organic Geochemistry, 16, 601–608.

Landis, C.A. (1971) Graphitization of dispersed carbonaceous material in metamorphic rocks. Contributions to Mineralogy and Petrology, 30, 34–45.

Lespade, P., Al-Jishi, R., and Dresselhaus, M.S. (1982) Model for Raman scattering from incompletely graphitized carbons. Carbon, 20, 427–431.

Lespade, P., Marchand, A., Couzi, M., and Cruege, F. (1984) Caractérisation de matériaux carbonés par microspectrométrie Raman. Carbon, 22, 375–385.

Macklin, J., Brownlee, D., Chang, S., and Bunch, T. (1990) Raman spectroscopic studies of carbon in extra-terrestrial materials. In J.C. Tarter, S. Chang, and D.J. DeFrees, Eds., Carbon in the galaxy: Studies from Earth and space, p. 336. NASA Conference Publication, 3061, Washington, DC.

Mildner, D.F.R., and Carpenter, J.M. (1982) On the short range atomic structure of non-crystalline carbon. Journal of Non-Crystalline Solids, 47, 391–402.

Miyashiro, A. (1964) Oxidation and reduction in the Earth's crust with special reference to the role of graphite. Geochimica et Cosmochimica Acta, 28, 717–729.

Morgan VI, G.B., Chou, I.-M., Pasteris, J.D., and Olsen, S.N. (1993) Re-equilibration of CO_2 fluid inclusions at controlled hydrogen fugacities. Journal of Metamorphic Geology, 11, 155–164.

Mosher, S., Burks, R.J., and Reck, B.H. (1987) Alleghenian deformation in the southern Narragansett Basin, Rhode Island. In D.C. Roy, Ed., Geological Society of America centennial field guide, northeastern section, 5, 191–194.

Murray, D.P. (1987) The Alleghenian orogeny in the Narragansett Basin area, Rhode Island. In D.C. Roy, Ed., Geological Society of America centennial field guide, northeastern section, 5, 187–190.

Nakamizo, M., Kammereck, R., and Walker, P.L. (1974) Laser Raman studies on carbons. Carbon, 12, 259–267.

Nakamizo, M., Honda, H., and Inagaki, M. (1978) Raman spectra of ground natural graphite. Carbon, 16, 281–283.

Nemanich, R.J., and Solin, S.A. (1979) First- and second-order Raman scattering from finite-size crystals of graphite. Physical Review B, 20, 392–401.

Oberlin, A., Boulmier, J.L., and Villey, M. (1980) Electron microscopic study of kerogen microtexture: Selected criteria for determining the evolution path and evolution stage of kerogen. In B. Durand, Ed., Kerogen—Insoluble organic matter from sedimentary rocks, p. 191–241. Editions Technip, Paris.

Oh, J.H., Rouzaud, J.N., Oberlin, A., Deurbergue, A., and Kwak, Y.H. (1991) Structural study of graphitization in the Moongyeong Coalfield, South Korea. Bulletin Société Geologique de France, 162, 399–407.

Okuyama-Kusunose, Y., and Itaya, T. (1987) Metamorphism of carbonaceous material in the Tono contact aureole, Kitakami Mountains, Japan. Journal of Metamorphic Geology, 5, 121–139.

Pasteris, J.D. (1988) Secondary graphitization in mantle-derived rocks. Geology, 16, 804–807.

———(1989) In situ analysis in geological thin-sections by laser Raman microprobe spectroscopy: A cautionary note. Applied Spectroscopy, 43, 567–570.

Pasteris, J.D., and Wanamaker, B.J. (1988) Laser Raman microprobe analysis of experimentally reequilibrated fluid inclusions in olivine: Some implications for mantle fluids. American Mineralogist, 73, 1074–1088.

Pasteris, J.D., and Wopenka, B. (1991) Raman spectra of graphite as indicators of degree of metamorphism. Canadian Mineralogist, 29, 1–9.

Pasteris, J.D., Kuehn, C.A., and Bodnar, R.J. (1986) Applications of the laser Raman microprobe RAMANOR U-1000 to hydrothermal ore deposits: Carlin as an example. Economic Geology, 81, 915–930.

Pasteris, J.D., Wopenka, B., and Seitz, J.C. (1988) Practical aspects of quantitative laser Raman microprobe spectroscopy for the study of fluid inclusions. Geochimica et Cosmochimica Acta, 52, 979–988.

Pearson, D.G., Boyd, F.R., Field, S.W., Pasteris, J.D., Haggerty, S.E., and Nixon, P.H. (1991) Graphite-bearing peridotites from Kaapvaal Craton: Their carbon isotopic compositions and implications for peridotite thermobarometry. In S.E. Haggerty and P.H. Nixon, Eds., Extended abstracts volume for the 5th international kimberlite conference, Araxa, Brazil, p. 323–325. Companhia de Pesquisa de Recursos Minerais, Brasilia, Brazil.

Reutel, C. (1992) Krustenfluide in Gesteinen und Lagerstätten am Westrand der Böhmischen Masse. Göttinger Arbeiten zur Geologie und Paläontologie nr. 53, p. 1–86. Selbstverlag der Geologischen Institute der Georg-August-Universität Göttingen, Göttingen, Germany.

Ross, J.V., and Bustin, R.M. (1990) The role of strain energy in creep graphitization of anthracite. Nature, 343, 58–60.

Rouzaud, J.N., Oberlin, A., and Beny-Bassez, C. (1983) Carbon films: Structure and microtexture (optical and electron microscopy, Raman spectroscopy). Thin Solid Films, 105, 75–96.

Rouzaud, J.N., Guechchati, N., Kister, J., and Conrad, J. (1991) Structural characterization of coalification: Example of Gironville Borehole. Bulletin de la Société Géologique de France, 162, 201–209.

Rumble III, D., and Hoering, T.C. (1986) Carbon isotope geochemistry of graphite vein deposits from New Hampshire, USA. Geochimica et Cosmochimica Acta, 50, 1239–1247.

Rumble III, D., Hoering, T.C., and Grew, E.S. (1977) The relation of carbon isotopic composition to graphitization of carbonaceous materials from the Narragansett Basin, Rhode Island. Carnegie Institution of Washington Year Book, 76, 623–625.

Sassani, D.C., and Pasteris, J.D. (1988) Preliminary investigation of alteration in a basal section of the southern Duluth Complex, Minnesota, and the effects on the oxide and sulfide mineralization. In K. Kisvarsanyi and S.K. Grant, Eds., Proceedings of the North American conference on tectonic control of ore deposits and vertical and horizontal extent of ore systems, p. 280–291. University of Missouri, Rolla, Missouri.

Seitz, J.C., Pasteris, J.D., and Wopenka, B. (1987) Characterization of CO_2-CH_4-H_2O fluid inclusions by microthermometry and laser Raman microprobe spectroscopy: Inferences for clathrate and fluid equilibria. Geochimica et Cosmochimica Acta, 51, 1651–1664.

Sterner, S.M., and Bodnar, R.J. (1984) Synthetic fluid inclusions in natural quartz. I. Compositional types synthesized and applications to experimental geochemistry. Geochimica et Cosmochimica Acta, 48, 2659–2668.

Tarter, J.C., Chang, S., and DeFrees, D.J., Eds. (1990) Carbon in the galaxy: Studies from Earth and space, p. 1–343. NASA Conference Publication, 3061, Washington, DC.

Thompson, J.B., and Norton, S.A. (1968) Paleozoic regional metamorphism in New England and adjacent areas. In E-an Zen, W.S. White, J.B. Hadley, and J.B. Thompson, Eds., Studies of Appalachian geology—Northern and maritime, p. 319–327. Interscience, New York.

Tissot, B.P., and Welte, D.H. (1984) Petroleum formation and occurrence, p. 1–627. Springer-Verlag, New York.

Tsu, R., Gonzalez, H., and Hernandez, I. (1978) Observation of splitting of the E_{2g} mode and two-phonon spectrum in graphites. Solid State Communications, 27, 507–510.

Tuinstra, F., and Koenig, J.L. (1970a) Raman spectrum of graphite. Journal of Chemical Physics, 53, 1126–1130.

——— (1970b) Characterization of graphite fiber surfaces with Raman spectroscopy. Journal of Composite Materials, 4, 492–499.

Valley, J.W., and O'Neil, J.R. (1981) $^{13}C/^{12}C$ exchange between calcite and graphite: A possible thermometer in Grenville marbles. Geochimica et Cosmochimica Acta, 45, 411–419.

Vidano, R., and Fischbach, D.B. (1978) New lines in the Raman spectra of carbons and graphite. Journal of the American Ceramic Society, 61, 13–17.

Wang, A., Dhamelincourt, P., Dubessy, J., Guerard, D., Landais, P., and Lelaurain, M. (1989) Characterization of graphite alteration in an uranium deposit by micro-Raman spectroscopy, x-ray diffraction, transmission electron microscopy and scanning electron microscopy. Carbon, 27, 209–218.

Wedeking, K.W., and Hayes, J.M. (1983) Carbonization of Precambrian kerogens. In M. Bjoroy, Ed., Advances in geochemistry 1981, p. 546–553. Wiley, Chichester, U.K.

Wintsch, R.P., O'Connell, A.F., Ransom, B.L., and Wiechmann, M.J. (1981) Evidence for the influence of f_{CH_4} on the crystallinity of disseminated carbon in greenschist facies rocks, Rhode Island, USA. Contributions to Mineralogy and Petrology, 77, 207–213.

Wopenka, B. (1988) Raman observations on individual interplanetary dust particles. Earth and Planetary Science Letters, 88, 221–231.

Wopenka, B., and Pasteris, J.D. (1988) "Graphites" in geological samples: Raman spectroscopic misfits? In D.E. Newbury, Ed., Microbeam analysis—1988, p. 196–200. San Francisco Press, San Francisco.

Wopenka, B., Pasteris, J.D., Bernatowicz, T.J., Dunn, S.R., and Valley, J.W. (1988) Si-bearing graphite from Tudor Township, Ontario. Eos, 69, 65.

Zen, E-an (1981) Metamorphic mineral assemblages of slightly calcic pelitic rocks in and around the Taconic allochthon, southwestern Massachusetts and adjacent Connecticut and New York. U.S. Geological Survey Professional Paper, 1113, 128 p.

Ziegenbein, D. (1979) Graphit in C-H-O Gasphasen: Experimentelle Untersuchung der Redox-Bedingungen in Gegenwart von fehlgeordnetem Graphit. Fortschritte der Mineralogie, 57, Beiheft 1, 165.

Ziegenbein, D., and Johannes, W. (1980) Graphite in C-H-O fluids: An unsuitable compound to buffer fluid composition at temperatures up to 700 °C. Neues Jahrbuch für Mineralogie Monatshefte, 7, 289–305.

——— (1990) Graphit-Fluid-Wechselwirkungen: Einfluß der Graphitkristallinität. Kontinentales Tiefbohrprogramm der Bundesrepublik Deutschland, Report 90-4, p. 559.

Zinner, E., Wopenka, B., Amari, S., and Anders, E. (1990) Interstellar graphite and other carbonaceous grains from Murchison meteorite: Structure, composition and isotopes of C, N, and Ne. Lunar and Planetary Science, 21, 1379–1380.

Manuscript received February 10, 1992
Manuscript accepted January 25, 1993